

# APPROXIMATE BAYESIAN INFERENCE OF DIRECTED ACYCLIC GRAPHS IN BIOLOGY WITH FLEXIBLE PRIORS ON EDGE STATES

BY EVAN A MARTIN<sup>1</sup> AND AUDREY QIUYAN FU<sup>2,a</sup>

<sup>1</sup>*The Bioinformatics and Computational Biology Program, University of Idaho*

<sup>2</sup>*The Bioinformatics and Computational Biology Program,  
Department of Mathematics and Statistical Science,  
Institute for Modeling Collaboration and Innovation,  
Institute for Interdisciplinary Data Sciences, University of Idaho*, <sup>a</sup>[audreyf@uidaho.edu](mailto:audreyf@uidaho.edu)

Graphical models or networks describe the statistical dependence among multiple variables and are widely used in biology (e.g., gene regulatory networks). Under appropriate assumptions, directed edges may represent causal relationships. A key feature of a biological network is sparsity, defined by how likely an edge is present, of which we often have some knowledge. However, most existing Bayesian methods use priors for the entire graph, making it difficult to specify the level of sparsity. The few methods that use priors on edges estimate the two directions independently; the sum of the two probabilities can exceed 1. Here, we present baycn (BAYesian Causal Network), a novel approximate Bayesian method that represents a graph in terms of three states of edges: the two directions and edge absence, and specifies priors on these edge states. We design a pseudo Bayesian sampling algorithm for efficient inference. We apply baycn to two genomic problems: i) distinguishing direct and indirect target genes of genetic variants, using these variants as instrumental variables, and ii) inferring combinatorial binding of highly-correlated transcription factors in *Drosophila*. In both cases and in extensive simulations, our method demonstrates much improved accuracy over existing methods for the whole graph and for individual edges.

Graphical models (or networks), which may include directed and undirected edges, can be used to represent the statistical dependence among multiple variables and have wide applications in biology, such as gene regulatory networks (Friedman, 2004; Rau et al., 2012) and protein-protein interaction networks (Gomez, Noble and Rzhetsky, 2003; Zhang et al., 2012). Under appropriate assumptions, directed edges in a network may represent causal (or regulatory) relationships (Spirtes, Glymour and Scheines, 2000; Guyon, Janzing and Schölkopf, 2010; Dawid, 2010) (also see Discussion).

A key feature of graphs is their sparsity, which measures how many edges are present in a graph, or how likely an individual edge is expected to be present. We often have some knowledge about the sparsity of a graph, especially in biology where it remains a challenge to infer a reliable gene regulatory network due to complexity in biological processes and high dimension of biological variables involved (McGuire et al., 2020; Davidson, 2010). For example, Guelzim et al. (2002) estimated that there are about 6000 genes in the yeast genome, and that on average each gene is regulated by only 2.76 regulators (such as transcription factors), meaning that the probability of edge presence in the graph is around 2.76/6000 a priori. This example shows that we describe sparsity more easily at the edge level than for the whole graph, and that it is often of interest to infer the probability of a state of an edge: the two directions if present, and absence.

---

*Keywords and phrases:* directed acyclic graphs, sparsity, priors on edge states, causal inference, gene regulatory networks.

Directed acyclic graphs (DAGs), often also called Bayesian networks, are graphs with only directed edges and no directed cycles. Many Bayesian methods have been developed for DAG inference, which explore the graph space and draw a sample graph, either directly from a closed-form posterior distribution (Schwaller, Robin and Stumpf, 2019; Leday and Richardson, 2019; Yeung et al., 2011; Lo et al., 2012; Young, Raftery and Yeung, 2014; Fronczuk, Raftery and Yeung, 2015; Hung et al., 2017) or more often use a Markov Chain Monte Carlo (MCMC) algorithm (Madigan, York and Allard, 1995; Friedman and Koller, 2003; Giudici and Castelo, 2003; Grzegorzczak and Husmeier, 2008; He et al., 2013; Mohammadi et al., 2015; Goudie and Mukherjee, 2016; Su and Borsuk, 2016; Kuipers and Moffa, 2017; Castelletti and Consonni, 2019; Rezaei Tabar et al., 2019; Viinikka and Koivisto, 2020; Castelletti and Consonni, 2020; Kuipers, Suter and Moffa, 2022; Castelletti and Peluso, 2022; Castelletti and Mascaro, 2022) to sample the posterior distribution.

Most of these methods estimate the probabilities for edge directions and absence, although the priors are typically for all DAGs or for node orderings/partitions (Madigan, York and Allard, 1995; Goudie and Mukherjee, 2016; Friedman and Koller, 2003; Su and Borsuk, 2016; Kuipers and Moffa, 2017; Rezaei Tabar et al., 2019; Viinikka and Koivisto, 2020; Castelletti and Consonni, 2020; Kuipers, Suter and Moffa, 2022). Such priors do not translate easily to priors on the states of an individual edge. For example, a uniform prior is often assumed for all the DAGs in these methods. In principle, one can calculate the overall probability of edge presence versus absence, dividing the total number of edges in all DAGs by the number of DAGs. The probability of each direction is then half the probability of edge presence. However, this calculation is not trivial, as the total number of DAGs is generally difficult to obtain. An exception is Castelletti and Peluso (2022), which constructed an edge-level prior as a proxy for the prior on the entire graph.

Several methods estimate the probability of the two directions, but only for the edges that are deemed present (Yeung et al., 2011; Lo et al., 2012; Young, Raftery and Yeung, 2014; Hung et al., 2017). In particular, Young, Raftery and Yeung (2014) used the prior above on gene regulators in their scanBMA method for gene expression data (see Section 1.3). However, the probability of edge absence is not directly calculated. The posterior probabilities of the two possible directions are also treated as independent of each other. As a result, both probabilities can sum to above 1.

In our development, we formulate priors by considering three states for an edge: two directions and edge absence. We introduce a new Bayesian method that substantially improves the prior specification and estimates the posterior probabilities of three possible states of an edge. We represent a Bayesian network by specifying the graph in terms of the edge states (i.e., two directions and edge absence). This framework allows the user to specify a prior distribution for the edge states, which is easier to formulate with biological information and to specify the level of sparsity in the graph. We take a pseudo Bayesian approach to designing the sampling algorithm for efficient inference. To reduce the size of the search space and speed up inference, our method can further take as input a graph from another more efficient graph inference method, e.g., constraint-based methods such as Badsha, Martin and Fu (2021); Kalisch et al. (2012) and Scutari (2010).

When instrumental variables are available, our method may be used for inferring causal networks. In genetics, for example, a genetic variant (denoted  $T_1$ ) regulating the expression of a gene ( $T_2$ ) can be used as an instrumental variable to better understand the regulatory relationships among genes, as the genotypes of individuals in a natural population are randomized. If the expression of another gene  $T_3$  tracks (i.e., is associated with) the changes in  $T_2$ , and if no other processes can explain such "tracking" (i.e., no confounding variables), then  $T_2$  is the cause of  $T_3$ ; in other words, this reasoning leads to the inference of a small graph  $T_1 \rightarrow T_2 \rightarrow T_3$ . This is the essence of the principle of Mendelian randomization (Davey Smith

and Hemani, 2014; Emdin, Khera and Kathiresan, 2017; Badsha and Fu, 2019). When instrumental variables are available and confounding variables are appropriately accounted for, this principle translates to a constraint in network inference, which requires the edge connecting the variant and the gene to point only to the gene, and not the other way around (Badsha and Fu, 2019; Badsha, Martin and Fu, 2021). Our method allows for this constraint, which often greatly reduces the graph space, and makes it possible to orient other edges.

We demonstrate the performance of our method through extensive simulation and in two biological applications. The first application examines the regulatory relationships among the target genes of genetic variants, while accounting for confounding variables in the inference. The second application disentangles combinatorial transcription factor binding during *Drosophila* mesoderm development, using a dataset with known edges supported by numerous biological experiments. In both cases, our method demonstrates much improved accuracy over existing methods.

## 1. Methods.

1.1. *A Bayesian graphical model for edge states.* A graph  $\mathcal{G} = (\mathbf{V}, \mathbf{E})$  is a set of vertices (nodes)  $\mathbf{V} = \{1, 2, \dots, b\}$  and edges  $\mathbf{E} \subseteq \mathbf{V} \times \mathbf{V}$ , where  $\mathbf{V} \times \mathbf{V}$  is the set of all ordered pairs of nodes, such as  $(j, k)$ , which denotes an edge pointing from node  $j$  to node  $k$  where  $j, k \in \mathbf{V}$ . The structure (or topology) of the graph is typically defined by the (deterministic) adjacency matrix  $\mathbf{A}$  of dimension  $b \times b$ , where  $A_{jk} = 1$  and  $A_{kj} = 0$  represent the edge  $j \rightarrow k$ , and  $A_{jk} = 0$  and  $A_{kj} = 1$  represent  $k \rightarrow j$ . If  $A_{jk} = A_{kj} = 0$ , there is no edge between nodes  $j$  and  $k$ .

We introduce baycn (BAYesian Causal Network), an alternate representation of the graph to directly describe the states of individual edges with the vector  $\mathbf{S} = (S_1, S_2, \dots, S_m)$ , where  $m$  is the number of edges. Note that the single subscript here denotes the index of the edge. An edge between nodes  $j$  and  $k$  (without loss of generality, we will assume  $j < k$ ) is in state  $S_i$ , which can take on three values:  $S_i = 0$  if  $j \rightarrow k$ ,  $S_i = 1$  if  $k \rightarrow j$ , and  $S_i = 2$  if the edge is absent. The edge state probability is then  $p_s \equiv \Pr(S_i = s)$  and  $\sum_{s=0}^2 p_s = 1$ . If  $p_0 = p_1 = 0.5$ , we consider the edge bidirected with both directions being equally likely.

When we want to emphasize the two nodes of an edge, we use the notation  $S_{jk}$  with the double subscript for nodes  $j$  and  $k$ . This notation allows us to connect the edge vector with the adjacency matrix, which is defined on the nodes:  $\Pr(S_{jk} = 0) = \Pr(A_{jk} = 1)$ ,  $\Pr(S_{jk} = 1) = \Pr(A_{kj} = 1)$ , and  $\Pr(S_{jk} = 2) = 1 - \Pr(A_{jk} = 1) - \Pr(A_{kj} = 1)$ .

When data is available at all the  $b$  nodes, we denote the data as  $\mathbf{T} = (T_1, T_2, \dots, T_b)^T$ , where each  $T_j$  represents the random variable at node  $j$ . We aim to infer the posterior edge state probability  $\Pr(S_i | \mathbf{T})$  for all edges. The posterior probabilities of the three states for an edge also add up to 1. We can also represent these posterior probabilities in a probabilistic adjacency matrix, where each entry is the probability of one of the two possible directions:  $\Pr(S_{jk} = 1 | \mathbf{T})$  or  $\Pr(S_{kj} = 1 | \mathbf{T})$ . Existing Bayesian methods generally produce such a posterior probabilistic adjacency matrix.

Edge state probabilities need to account for Markov equivalence. Two graphs are Markov equivalent if they have the same likelihood and represent the same conditional independence (Verma and Pearl, 1990). A set of Markov equivalent graphs form a Markov equivalence class. For example, the canonical mediation model of  $T_1 \rightarrow T_2 \rightarrow T_3$  has two Markov equivalent graphs:  $T_1 \leftarrow T_2 \rightarrow T_3$ , and  $T_1 \leftarrow T_2 \leftarrow T_3$  (Figure 1A). All three graphs depict marginal dependence between  $T_1$  and  $T_3$  (i.e.,  $T_1 \not\perp T_3$ ) and conditional independence given  $T_2$  (i.e.,  $T_1 \perp T_3 | T_2$ ). Accounting for these Markov equivalent graphs, the true edge state probabilities are  $(0.33, 0.67, 0)$  for the edge  $T_1 \rightarrow T_2$  and  $(0.67, 0.33, 0)$  for  $T_2 \rightarrow T_3$ . In contrast, the graph  $T_1 \rightarrow T_2 \leftarrow T_3$  (Figure 1B), also known as a v-structure, represents marginal independence between  $T_1$  and  $T_3$  and their conditional dependence ( $T_1 \not\perp T_3 | T_2$ ). This graph has no Markov equivalent graphs, and the true edge state probabilities are either 0 or 1.

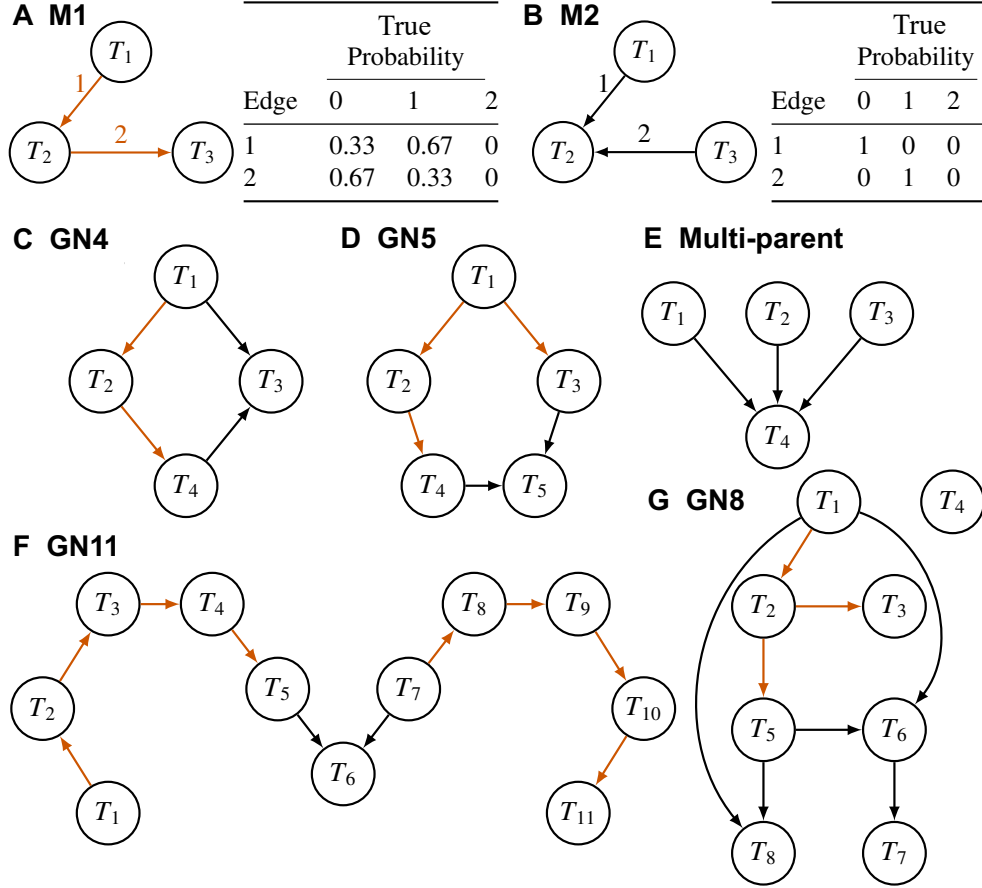


Fig 1: **Seven topologies used in simulation studies.** Orange edges have Markov equivalent edges and cannot be deterministically inferred. (A) A mediation model where  $T_2$  is the mediator. (B) A v-structure. True probabilities on edge states account for Markov equivalence. The values show the existence of Markov equivalent graphs for M1 and no Markov equivalent graphs for M2. (C)-(G) Larger networks that contain M1 and M2 as subgraphs. See Supplementary Figures S1-S7 for the true edge state probabilities of the orange edges.

The probability of the graph can be written as a product of conditional probabilities where each node is conditioned on its parents

$$(1) \quad \Pr(\mathbf{T} | \mathbf{S}, \boldsymbol{\theta}) = \prod_{j=1}^b \Pr(T_j | pa(T_j), \boldsymbol{\theta}_j),$$

where  $pa(T_j)$  is the set of parent nodes of  $T_j$ ,  $\boldsymbol{\theta}_j$  is the parameter vector for the distribution of  $T_j$ . When  $pa(T_j) = \emptyset$ , where  $\emptyset$  is an empty set, the probability is reduced to a marginal probability  $\Pr(T_j | \boldsymbol{\theta}_j)$ .

When we assume normality for the data at each node:

$$(2) \quad T_j \sim \mathcal{N}(\mu_j, \sigma_j^2), \text{ and } \mu_j = \beta_{0j} + \sum_{k \in pa(T_j)} \beta_{kj} T_k,$$

where  $\mu_j$  is the mean and  $\sigma_j^2$  the variance. If there are no parents,  $\mu_j = \beta_{0j}$ .

Alternatively, if the data is binary:

$$(3) \quad T_j \sim \text{Bernoulli}(p_j), \text{ and } \log\left(\frac{p_j}{1-p_j}\right) = \beta_{0j} + \sum_{k \in \text{pa}(T_j)} \beta_{kj} T_k,$$

where  $p_j$  is the ‘‘success’’ probability. Without parents,  $\log[p_j/(1-p_j)] = \beta_{0j}$ .

1.2. *The prior distribution and a Metropolis-Hastings-like iterative algorithm using pseudo-likelihood.* We aim to develop an iterative sampler that proposes changes to edge states and estimates the posterior probabilities, while accounting for Markov equivalence. Since our interest here is in learning the graph structure, but not the means and variances of the effect sizes of the parent nodes on their child nodes, we view the parameters represented by  $\theta$  (as in Equation 1) as nuisance parameters. This means that we are interested in the posterior distribution only for  $\mathbf{S}$ :  $\Pr(\mathbf{S}|\mathbf{T}) \propto \Pr(\mathbf{T}|\mathbf{S})\Pr(\mathbf{S})$ , in which the likelihood  $\Pr(\mathbf{T}|\mathbf{S})$  of the current graph involves  $\theta$ . Bayesian methods using pseudo-likelihoods, such as conditional, marginal, and profile likelihoods, have been widely used for elimination of nuisance parameters in a computationally efficient way (see the reviews in [Ventura and Racugno \(2016\)](#) and [Severini \(2000\)](#), although [Ventura and Racugno \(2016\)](#) considers such methods ‘‘hybrid/quasi/pseudo Bayesian’’ methods and the posteriors ‘‘pseudo-posteriors’’). Here, we calculate the likelihood  $\Pr(\mathbf{T}|\mathbf{S})$  by plugging the maximum likelihood estimates of  $\theta$  for the given graph into Equation 1. As a result, we call our sampler a ‘‘Metropolis-Hastings-like iterative algorithm’’. We demonstrate through simulations the accuracy and computational efficiency of this algorithm.

To infer the posterior of  $\Pr(\mathbf{S}|\mathbf{T})$ , we will use a prior that assumes all the edges to be independent:  $\Pr(\mathbf{S}) = \prod_m \Pr(S_i = s_i)$ . We can construct the prior based on our knowledge or belief on graph sparsity. For example, as mentioned in the Introduction, in the yeast genome we expect the prior probability for each direction to be  $2.76/6000/2$ , and that for edge absence to be  $1-2.76/6000$ . Once the probabilities for each edge are specified, we can multiply the probabilities of all the edges as in the equation above to obtain the probability of all the edges. Although the construction of  $\Pr(\mathbf{S})$  treats the edges independently, the posterior probabilities  $\Pr(\mathbf{S}|\mathbf{T})$  account for the dependence among the edges through the likelihood. Such a prior is easy to construct: for example, in biology one can easily find information on the mean number of connections certain genes may have. A similar prior has been used in the scanBMA method ([Young, Raftery and Yeung, 2014](#)); see Section 1.3.

The input of our algorithm is the binary adjacency matrix of a candidate graph and the data at the nodes. The candidate graph may be a fully connected graph, where all nodes are connected. A more efficient approach is to run a fast graph inference algorithm to produce a candidate graph and use it as the input, even if this graph contains false edges.

At the  $t$ th iteration, the key steps of the Metropolis-Hastings-like algorithm are:

1. Generate a proposal graph  $\mathbf{S}'_{(t)}$  from the current graph  $\mathbf{S}_{(t-1)}$ . When  $t = 1$ , the current graph is randomly generated from the candidate graph in the input.
2. Check for and remove directed cycles in  $\mathbf{S}'_{(t)}$ .
3. Calculate the acceptance probability  $\alpha_{(t)}$

$$(4) \quad \alpha_{(t)} = \min \left\{ \frac{\Pr(\mathbf{S}'_{(t)}) \Pr(\mathbf{T} | \mathbf{S}'_{(t)}, \theta_{(t)}) \Pr(\mathbf{S}_{(t-1)} | \mathbf{S}'_{(t)})}{\Pr(\mathbf{S}_{(t-1)}) \Pr(\mathbf{T} | \mathbf{S}_{(t-1)}, \theta_{(t-1)}) \Pr(\mathbf{S}'_{(t)} | \mathbf{S}_{(t-1)})}, 1 \right\},$$

where  $\Pr(\mathbf{S})$  is the prior probability of the edge states,  $\Pr(\mathbf{T} | \mathbf{S}, \theta)$  the graph likelihood, and  $\Pr(\mathbf{S} | \mathbf{S}')$  the transition probability. Here, we estimate  $\theta$  by maximum likelihood estimation in the corresponding graph.

4. Generate a random probability  $u$  from the uniform distribution  $U(0, 1)$ . Accept the proposal and set  $\mathbf{S}_{(t)} = \mathbf{S}'_{(t)}$  if  $u < \alpha_{(t)}$ ; or stay at the current graph and set  $\mathbf{S}_{(t)} = \mathbf{S}_{(t-1)}$  otherwise.

To generate the proposal graph in step 1, we first determine the number of edges to change states by sampling from a binomial distribution  $\text{Bin}(m, 1/m)$ , where  $m$  is the number of edges in the network and  $1/m$  is then the “success” probability. For each of the selected edges, we then sample from a Bernoulli distribution with probability  $p$  to decide which edge state to change to. Since we do not allow for an edge to remain in the same state,  $p$  is determined by the prior of the two remaining edge states. For example, if an edge in state 0 is selected to change states, and if the prior probability for the edge states is  $(p_0, p_1, p_2) = (0.05, 0.05, 0.9)$ , then the probability of switching to state 1 is  $p = 0.05/(0.05 + 0.9)$ .

To ensure that the proposal graph does not contain directed cycles, we have further designed two algorithms as part of our algorithm (Supplementary Note S1): the “cycle finder” algorithm finds all possible cycles given the input graph; and the “cycle remover” algorithm removes all directed cycles from the proposal graph.

The binomial and Bernoulli probabilities above are then used to calculate the transition probability in step 3. We show that the transition probabilities do not depend on the path taken from the current graph to the proposed graph (the process of introducing and removing directed cycles) but only on the edges that have different states between the two graphs (see the proof in Supplementary Note S2 and examples in Supplementary Note S3):

**THEOREM 1.** *When calculating the acceptance probability, the transition probabilities between the current graph  $\mathbf{S}$  and proposed graph  $\mathbf{S}'$ ,  $\Pr(\mathbf{S}'|\mathbf{S})$  and  $\Pr(\mathbf{S}|\mathbf{S}')$ , depend only on the edges whose states are different between the two graphs.*

This algorithm generates a sample of graphs represented by edge states (Figure 2). For each edge, the relative frequencies of the three states in the sample provide an estimate of the marginal posterior probabilities of edge states  $\Pr(S_i | \mathbf{T})$ , marginalized across the sampled DAGs.

Through changes in edge states, our algorithm can sample from multiple Markov equivalent graphs and thus produce posterior probabilities that account for Markov equivalence. With sufficient data, the posterior probabilities of edge states should be the same asymptotically as expected under Markov equivalence.

In causal inference with instrumental variables, we need to restrict the direction of the edge connecting the instrumental variable and other nodes. Our algorithm achieves this by generating proposals with this restriction. For example, when the input is the undirected network  $T_1 - T_2 - T_3$ , it may imply four possible directed networks as mentioned earlier: i)  $T_1 \rightarrow T_2 \rightarrow T_3$ , ii)  $T_1 \leftarrow T_2 \leftarrow T_3$ , iii)  $T_1 \leftarrow T_2 \rightarrow T_3$ , and iv)  $T_1 \rightarrow T_2 \leftarrow T_3$ . If  $T_1$  is a potential instrumental variable, an edge between  $T_1$  and  $T_2$ , when existing, can point only to  $T_2$ . Then the possible directed networks are reduced to only i) and iv), which have different likelihoods and are therefore distinguishable. In this simple example, our algorithm can propose only two moves for the edge  $T_1 - T_2$  ( $T_1 \rightarrow T_2$ , and no edge) but three moves for the edge  $T_2 - T_3$  ( $T_2 \rightarrow T_3$ ,  $T_2 \leftarrow T_3$ , and no edge).



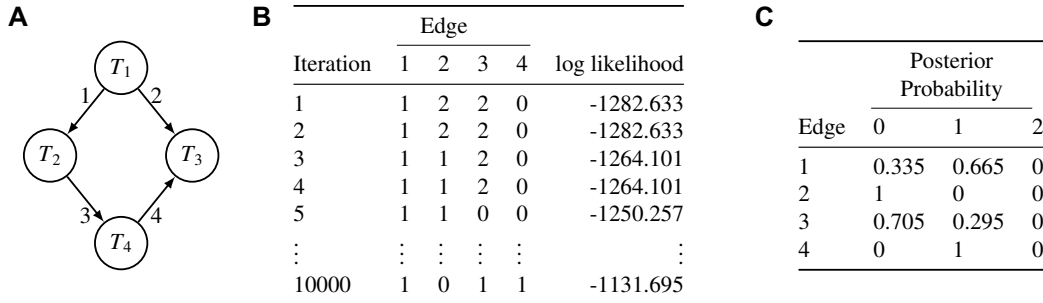


Fig 2: **An example of the output from baycn.** (A) The true graph GN4. The candidate graph used for inference will also consider only these four edges. (B) Edge states and log likelihood for the graph accepted at each iteration of the Metropolis-Hastings-like algorithm. (C) The proportion of each edge state in the sample provides an estimate of the posterior probability of the edge state.

1.3. *Relationship to existing Bayesian methods.* We compare baycn to five methods (Table 1), four of which are MCMC methods. Two methods are based on the graph structure: Gibbs (Goudie and Mukherjee, 2016) and MC<sup>3</sup> (Madigan, York and Allard, 1995), and two methods are based on node orderings or node partitions (i.e., subsets of nodes): order MCMC (Friedman and Koller, 2003; Kuipers, Suter and Moffa, 2022) and partition MCMC (Kuipers and Moffa, 2017; Kuipers, Suter and Moffa, 2022). These methods assign a prior for the entire graph or for the node ordering/partition.

TABLE 1  
**Summary of our method and other Bayesian methods for network inference.**

	baycn	Gibbs (Goudie and Mukherjee, 2016)	MC <sup>3</sup> (Madigan, York and Allard, 1995)	order MCMC (Friedman and Koller, 2003; Kuipers, Suter and Moffa, 2022)	partition MCMC (Kuipers and Moffa, 2017; Kuipers, Suter and Moffa, 2022)	scanBMA (Young, Raftery and Yeung, 2014)
Input	Data matrix, adjacency matrix, prior on edge states	Data matrix, edge list (optional), prior on graph space	Data matrix, edge list (optional), prior on graph space	Data matrix, edge list (optional), parameters for graph score	Data matrix, edge list (optional), parameters for graph score	Data matrix, prior for edge presence
Output	Posterior probabilities of three edge states	Posterior probabilistic adjacency matrix	Posterior probabilistic adjacency matrix	Posterior probabilistic adjacency matrix	Posterior probabilistic adjacency matrix	Posterior probabilities of parent nodes
Sampling space	Candidate edges and their direction	Parent nodes	Candidate edges and their direction	Node orderings	Node partitions	Parent nodes
Sampling steps	Change states for $>= 1$ edges	Change parents for $>= 1$ nodes	Add or remove an edge	Move a node to a new position	Split or merge existing partitions	Closed form for posterior
Type of prior	Edge states	Parameters and graph structure	Parameters and graph structure	Parameters and node orderings	Parameters and node partitions	Parameters and edges
Type of data	Discrete, continuous, or mixed	Discrete or continuous	Discrete or continuous	Discrete or continuous	Discrete or continuous	Continuous
R package	baycn	structmcmc	structmcmc	BIDAG	BIDAG	networkBMA



We also compare with scanBMA (Young, Raftery and Yeung, 2014), a Bayesian model averaging method that specifies a prior probability for individual edges (Yeung et al., 2011; Lo et al., 2012; Young, Raftery and Yeung, 2014). As mentioned in the Introduction, one of the priors assigns the same probability to all edges, and this probability is  $g_1/g_2$ , where  $g_1$  is the expected number of the regulators for any gene, and  $g_2$  the number of all possible regulators (they used 2.76/6000). They further allow for this probability to vary for different genes in another prior. scanBMA searches the space of parents for each node in the network independently. As a result, the two probabilities it estimates for the two directions are independent of each other and can sum to a value above 1. Additionally, it does not estimate the probability of edge absence.

1.4. *Simulation studies.* We simulated data under seven different topologies (Figure 1). Each node was simulated under a linear model in Equation 2 with the variance set to 1 and the intercept  $\beta_0$  set to 0. All the other coefficients take the same value, which is referred to as the signal strength. We considered three levels of the signal strength: 0.2 (weak), 0.5 (moderate), and 1 (strong), and three levels of the sample size: 100, 200 and 600. For each topology, we simulated 25 datasets under each of the nine combinations of signal strength and sample size. When summarizing the results, if the results are grouped by, for example, topology, we use the output from all the datasets with different sample sizes and signal strengths.

We evaluate the performance using the following metrics:

1. The edgewise Mean Squared Error (eMSE): This is the MSE between the true probabilities and posterior probabilities of the three states for edge  $i$ :

$$(5) \quad \text{eMSE}_i = \frac{1}{3} \sum_{s=0}^2 [\Pr(S_i = s)^{\text{true}} - \Pr(S_i = s | \mathbf{T})]^2,$$

where  $\Pr(S_i = s)^{\text{true}}$  is the true edge state probability under Markov equivalence. This metric informs us which edges are more accurately inferred and which ones are not. Note that the true probabilities can be calculated only when the structure of the true graph is known: we identify all possible graphs in the Markov equivalence class of the true graph, and then calculate the frequency of an edge being in each of the three states (see Supplementary Figures S1–S7).

2.  $\text{MSE}_1$ : This is the MSE for the whole graph based on three possible edge states. It is the eMSE averaged over all  $m$  edges in the graph:

$$(6) \quad \text{MSE}_1 = \frac{1}{m} \sum_{i=1}^m \text{eMSE}_i = \frac{1}{3m} \sum_{i=1}^m \sum_{s=0}^2 [\Pr(S_i = s)^{\text{true}} - \Pr(S_i = s | \mathbf{T})]^2.$$

3.  $\text{MSE}_2$ : This is the MSE between the true and posterior probabilistic adjacency matrices on all  $m$  edges. In other words, this metric uses the probability only of the two edge directions.

$$(7) \quad \text{MSE}_2 = \frac{1}{2m} \sum_{\substack{(j,k) \text{ or} \\ (k,j) \in \mathbf{E}}} \left\{ [\Pr(A_{jk} = 1)^{\text{true}} - \Pr(A_{jk} = 1 | \mathbf{T})]^2 \right. \\ \left. + [\Pr(A_{kj} = 1)^{\text{true}} - \Pr(A_{kj} = 1 | \mathbf{T})]^2 \right\}.$$

4. Precision and power for the whole graph. Precision, or  $1 - \text{False Discovery Rate (FDR)}$ , measures how many of the inferred edges are true, and power measures how many of the true edges are correctly inferred. For calculation, we apply a cutoff to the posterior probability of edge presence. These metrics ignore the nuances in the probabilities, but are easy to interpret and provide a quick indication of the inference accuracy.

## 2. Results.

### 2.1. Results from simulation studies.

#### 2.1.1. Estimating posterior probabilities of edge states using true edges as the input.

We ran baycn once per simulated dataset, used a burn-in of 20%, and used a sparse prior,  $(p_0, p_1, p_2) = (0.05, 0.05, 0.9)$ , on edge states. For M1, M2, GN4, GN5, and multi-parent topologies (Figure 1A-E), we ran baycn for 30,000 iterations with a step size of 120. For GN8 and GN11 (Figure 1F-G), we ran baycn for 50,000 iterations with a step size of 200.

As expected,  $MSE_1$  (based on three edge states) decreases as  $\beta$  and  $N$  increase for each topology, and is particularly affected by  $\beta$  (Supplementary Table ??). When  $MSE_1 < 0.1$ , the inference is typically accurate: the direction of each edge is correctly inferred, and the posterior probabilities of each edge state is similar to that of the true probabilities. Using this cutoff, we observed that baycn performs well in general when the signal strength is not weak. For both M2 and multi-parent topologies that only contain v-structures, however,  $MSE_1$  is much larger at  $\beta = 0.2$ . This is consistent with previous observation that it is generally difficult for existing graph inference algorithms to correctly identify v-structures with a weak signal (Badsha and Fu, 2019; Badsha, Martin and Fu, 2021).

#### 2.1.2. Identification of false positive edges and the choice of priors.

For this assessment we include a false edge in M1, M2 and GN4, and two false edges in GN11 (Supplementary Figure ??). We used the same data generated in the previous section for these topologies (without false edges) and ran baycn with the input being the true edges plus the false edges. The user can specify their prior belief on sparsity through the prior edge state probabilities. Here, we explored the impact of three edge state priors on the inference, with an increasing probability of edge absence: prior 1:  $(p_0, p_1, p_2) = (1/3, 1/3, 1/3)$ ; prior 2:  $(p_0, p_1, p_2) = (0.25, 0.25, 0.5)$ , and prior 3:  $(p_0, p_1, p_2) = (0.05, 0.05, 0.9)$ .

We calculated the eMSE for each edge and again used 0.1 as the cutoff. In all four graphs, the eMSE for the false edges decreases as  $p_2$  increases, but the edge probabilities of the true edges are generally estimated correctly, even when the false edges are not properly identified and have a large eMSE (Supplementary Tables ?? - S5). On the other hand, baycn can identify false positive edges under prior 3 (Supplementary Tables ?? - S5), confirming that prior 3 is the prior of choice, as it balances the need to detect false positive edges and correctly infer true edges.

#### 2.1.3. Comparison with existing Bayesian methods on simulated data.

To compare baycn with other methods, we focus on GN4, GN8 and GN11, which have different levels of complexity (Figure 1). Using the true edges as the input to all the methods, we ran each method for 30,000 iterations on GN4 and for 50,000 iterations on GN8 and GN11 and used a burn-in of 20%. We set the step size in baycn to 120 for GN4 and 200 for GN8 and GN11. We used the default step size for order and partition MCMC, which results in the step size being 30 for GN4 and 50 for GN8 and GN11. Gibbs and  $MC^3$  use all of the iterations after the burn-in.

Across topologies and simulation scenarios, baycn and Gibbs show similar and better performance than other methods (Figure 3; Supplementary Table S6). Partition and order MCMC are slightly worse in some cases, whereas  $MC^3$  is the least accurate and least stable among the MCMC methods (Figure 3).

$MSE_2$  (between the true and posterior probabilistic adjacency matrices) used in the comparison above does not apply to scanBMA, as the posterior probabilities from scanBMA have a different interpretation from the other methods (see Section 1.3). We therefore compare precision and power, in addition to  $MSE_2$ , on GN4 using a fully connected graph as the input

(Figure 4). To calculate precision and power, we applied a cutoff of 0.5 to the probability of edge presence for all methods and thus derived the binary inference (presence or absence) for each edge. Precision is nearly perfect for baycn and the MCMC methods in most simulations (Figure 4; Supplementary Table S7). However, scanBMA has lower precision under strong and moderate signal, mainly due to its inability to infer the v-structure. Power is nearly 1 for all methods at  $\beta = 0.5$  and 1 (Figure 4; Supplementary Table S7), but is lower at  $\beta = 0.2$ . Variation in power is larger for order and partition MCMC, as they tend to infer a higher posterior probability for edge absence (Supplementary Tables S8-S10). In terms of  $MSE_2$ , order MCMC has a large variability at weak signal, whereas Gibbs and  $MC^3$  are more variable at strong signal.

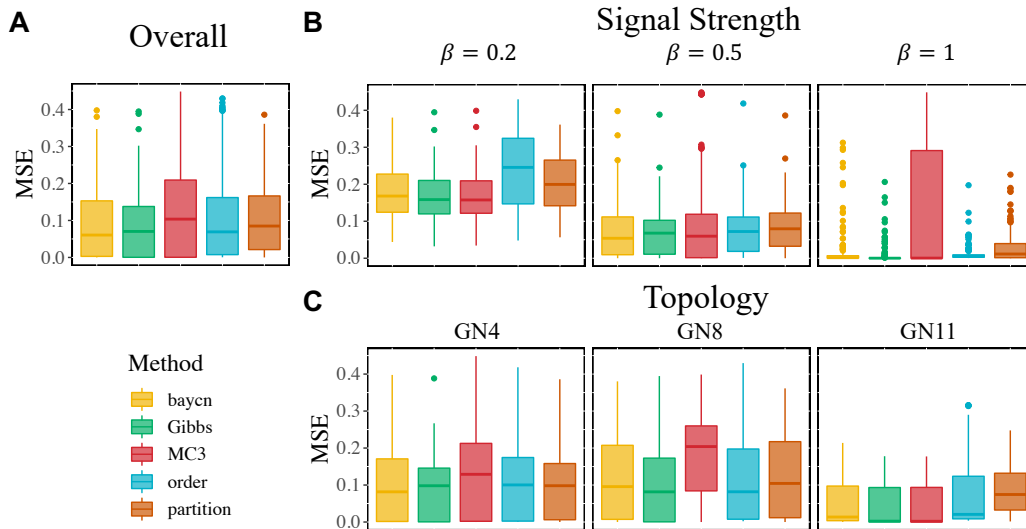


**Fig 3: Boxplots of  $MSE_2$  (on the posterior probabilistic adjacency matrix) for baycn and other Bayesian methods on simulated data from GN4, GN8, and GN11.** The true edges were used as the input to each method. **(A)** The overall  $MSE_2$  grouped by method. This plot combines the  $MSE_2$  for all topologies, signal strengths, and sample sizes. **(B)**  $MSE_2$  grouped by method and signal strength  $\beta$ . **(C)**  $MSE_2$  grouped by method and topology.

To compare the runtime of these methods, we ran each algorithm on an Intel Xeon D-1540 2.00 GHz processor with 128 GB of memory on data from GN4, GN8, and GN11 with  $\beta = 1$  and  $N = 600$  (Table 2). For all three topologies, scanBMA is the fastest, and Gibbs and  $MC^3$  the slowest. Order MCMC, partition MCMC and baycn are in the middle: they are an order of magnitude slower than scanBMA, but an order of magnitude faster than Gibbs and  $MC^3$ . Among these three methods in the middle, order MCMC is faster, whereas baycn and partition MCMC are similar. This comparison shows another advantage of baycn: apart from a more coherent framework, as well as improved accuracy and stability, baycn is also computationally efficient.

TABLE 2

**The mean runtime in seconds across 25 datasets.** For each topology, 25 datasets were generated with  $\beta = 1$  and  $N = 600$ . Each algorithm was run once per dataset, and the runtime in seconds was recorded. All algorithms were run on an Intel Xeon D-1540 2.00 GHz processor with 128 GB of memory.

Topology	Runtime (seconds)					
	baycn	Gibbs	MC <sup>3</sup>	order	partition	scanBMA
GN4	4.49	235.00	11.94	1.78	3.93	0.02
GN8	8.11	363.91	22.49	2.88	7.97	0.05
GN11	7.07	380.97	23.52	3.10	9.39	0.09

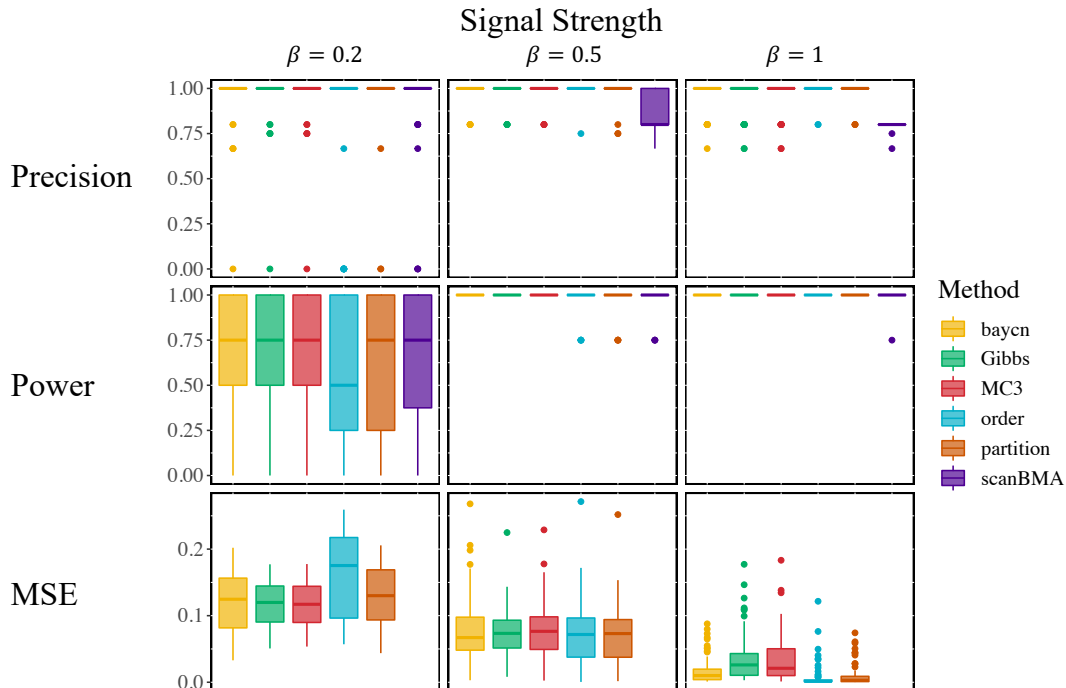


Fig 4: Boxplots of precision, power, and  $MSE_2$  (on the posterior probabilistic adjacency matrix) for baycn and other Bayesian methods on simulated data from GN4. A fully connected graph was used as the input to each method.  $MSE_2$  was not calculated for scanBMA, since the posterior probabilities from scanBMA have a different interpretation from the MCMC methods (see Section 1.3).

*2.2. Application: causal inference of transcription regulation with genetic variants.* Genetic variants play an important role in regulating gene expression (Cheung and Spielman, 2009). The GEUVADIS (Genetic European Variation in Disease) project identified a large number of variants that are associated with the expression of one or more genes in Lymphoblastoid Cell Lines (LCLs) in Europeans and Africans (Lappalainen et al., 2013). Among these variants, which are termed expression quantitative trait loci (eQTLs), 62 are associated with more than one gene. However, since the association analysis examined one eQTL-gene pair at a time, it is unclear which associated genes are more likely to be direct targets (i.e., having an edge with the variant), and which ones indirect targets (i.e., not having an edge with the variant).

To address this question, we infer graphs for these eQTL-gene sets, using each eQTL as an instrumental variable and applying the principle of Mendelian randomization (Sander-

son et al., 2022). Under this principle, an edge connecting an eQTL and a gene points only to the gene, but not the other way around, since the DNA (eQTL here) regulates the RNA (expression). We focus on the larger European sample of 373 individuals. The gene expression data in GEUVADIS had been normalized using the PEER method (Stegle et al., 2012) to remove potential impact of demographic variables, batch effect, and other covariates. To account for confounding from genes outside the small graph, we performed principal component analysis on the gene expression from all genes in the GEUVADIS data. We used Holm’s method to control the familywise type I error rate across all the p-values at 5% (Holm, 1979), and identified principal components (PCs) that are highly significantly associated with the eQTLs or genes in all the trios of that tissue. These PCs were then included in the network as confounding variables. The eQTL-gene sets Q8, Q21, Q23, Q37, and Q50 all have at least one PC associated with them while the eQTL-gene sets Q20 and Q62 do not have any PCs associated with them.

On each eQTL-gene-PC set, we used a fully connected graph as the input to baycn with a sparse prior  $(p_0, p_1, p_2) = (0.05, 0.05, 0.9)$ . We also included in baycn the constraint that a gene cannot be the parent of an eQTL. We ran baycn for 50,000 iterations with a burn-in of 20% and a step size of 200.

Based on the simulation results, we also ran order MCMC, partition MCMC, and scanBMA on the eQTL-gene set Q8 from GEUVADIS to compare with baycn (Figure 5). In all the methods, we used a fully connected graph as the input and applied the same constraint that a gene cannot be the parent of an eQTL. Since scanBMA allows for a prior on edges, we set the probability of edge presence to be 0.1, which is the same as our sparse prior for baycn. We ran each MCMC method for 30,000 iterations and used a burn-in of 20%. We set the posterior probability cutoffs for edge presence to be 0.5, and considered an edge directed if the difference between the posterior probabilities for the two directions is greater than 0.2.

Inferred graphs with the posterior probabilities are shown in Figure 5 (see tables of posterior probabilities for all edges in Supplementary Tables S11-S14). The inference from baycn, order MCMC and partition MCMC is similar for most of the edges (Figure 5A-C). However, order MCMC did not infer any edges involving the PCs, and partition MCMC inferred only one edge (RP11-203M5.8 - PC6) that has a relatively strong correlation of 0.25 (Figure 5E). Since the PCs were treated the same as the other nodes by these three methods, the results indicate that order and partition MCMC can identify only edges with strong correlations, and are insensitive to moderate and weak correlations. On the other hand, scanBMA is as sensitive to correlations as baycn is, but cannot infer edge absence or direction (Figure 5D).

The inference of the direction of the edge between PNP and RP11-203M5.8 is different under baycn and under order/partition MCMC (Figure 5A-C). This result is driven by PCs: when regressing RP11-203M5.8 on all the other variables, PC2 has a coefficient significantly different from 0 (p-value: 0.001), which means that RP11-203M5.8 and PC2 are conditionally dependent given other variables. Since they are both connected to PNP, this conditional dependence means that RP11-203M5.8 and PC2 are both parents of PNP, thus forming a v-structure:  $\text{RP11-203M5.8} \rightarrow \text{PNP} \leftarrow \text{PC2}$ . This is why baycn infers an edge from RP11-203M5.8 to PNP. To further verify the impact of PCs, we applied baycn to Q8, while excluding the PCs. This analysis led to the same inference as order/partition MCMC, which effectively ignored the PCs (Supplementary Table S15). These results demonstrate the importance of accounting for confounding variables and that of having sufficient sensitivity to the signals in data.

Analyses of all the eQTL-gene-PC sets show that baycn can identify the regulatory relationship among multiple genes associated with the same eQTL, while accounting for confounding variables (Supplementary Figures S9-S14; Supplementary Tables S16-S21). The posterior probabilities estimated by baycn are largely consistent with the sample correlations (Supplementary Figures S9-S14).

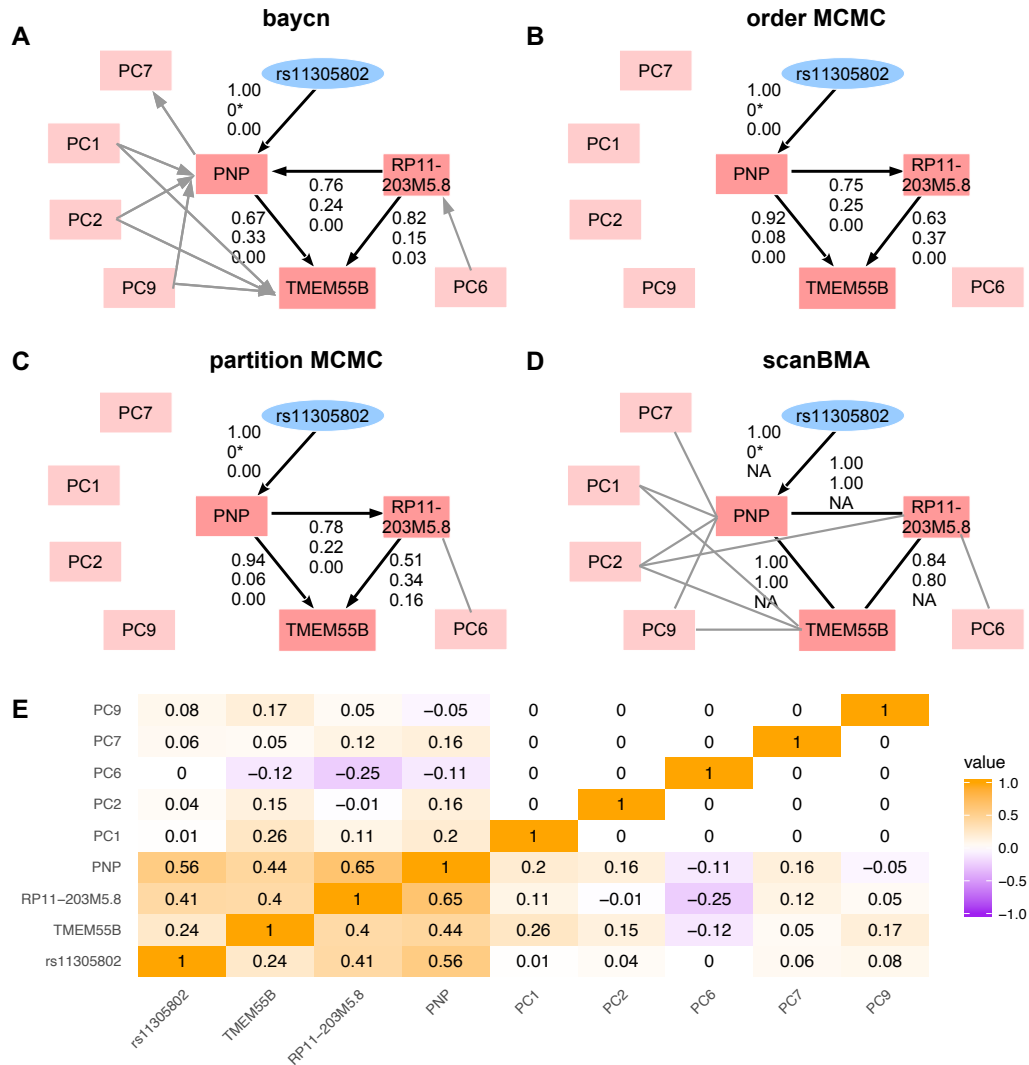


**Fig 5: Inference of the GEUVADIS eQTL-gene set Q8.** This eQTL is inferred to be associated with three genes. (A)-(D) Graphs inferred by different methods with posterior probabilities shown for edges of biological interest. The three probabilities are for the inferred direction shown in the figure, the opposite direction, and absence of the edge, respectively. For an undirected edge, the two posterior probabilities for direction are close. 0\* indicates that the directed edge pointing toward the eQTL was prohibited during inference. scanBMA is unable to infer the probability of edge absence (hence the NAs in (D)) or distinguish the two directions. (E) Heatmap of Pearson correlations in the data. The posterior probability of all the edges are in Supplementary Tables S11-S14.

**2.3. Application: inferring combinatorial binding of transcription factors.** Transcription factors (TFs) regulate the expression of target genes by combinatorial binding to regulatory sequences in the genome (Villar, Flicek and Odom, 2014). Here, we re-analyzed multiple highly-correlated TF binding profiles in 310 *cis*-regulatory regions known as *cis*-regulatory modules (CRMs) during early development in *Drosophila* (Zinzen et al., 2009) (Figure 6A). These TFs have a number of edges that are well supported by experimental evidence (Zinzen et al., 2009; Stojnic, Fu and Adryan, 2012), and the dataset was analyzed using a non-



Bayesian graphical model approach for each of six tissues (Stojnic, Fu and Adryan, 2012). This dataset consists of ChIP-chip binding profiles of five key TFs at two-hour intervals during mesoderm development in five tissue types in the embryos of *Drosophila melanogaster*: Twist (Twi), Tinman (Tin), Myocyte enhancing factor 2 (Mef2), Bagpipe (Bap), and Binou (Bin). The six tissue types are mesoderm (Meso), somatic muscle (SM), visceral muscle (VM), mesoderm and somatic muscle (Meso&SM), visceral muscle and somatic muscle (VM&SM). Because of repeated measurements over time and combinatorial binding, there exist strong correlations among these binding profiles, and most graph inference methods could not tell them apart and tended to infer a dense network (Stojnic, Fu and Adryan, 2012).

Whereas Stojnic, Fu and Adryan (2012) inferred a network for each tissue separately, here we applied baycn and inferred one network for the five tissues and five TFs. We first used a machine learning network inference method MRPC (Badsha and Fu, 2019; Badsha, Martin and Fu, 2021) to generate a candidate graph. Since MRPC tends to be conservative, we included in the candidate graph additional edges that could exist (Supplementary Figure S15). We ran baycn for 500,000 iterations with a burn-in of 0.2 and a step size of 800. An edge is considered present if the posterior probability of edge presence is greater than 0.5, and an edge is considered directed if the difference between the posterior probabilities for the two directions is greater than 0.2.

Our analysis showed that baycn can identify TFs known to drive tissue differentiation, even when the inference was performed for all the tissues together (Figure 6B; Supplementary Table S22). The inferred edges are consistent with the known relationships (Figure 6C). However, it is worth emphasizing that edges in a DAG represent conditional dependence. The inferred edge [Twi at 4-6h  $\rightarrow$  Twi at 2-4h] does not imply that later binding regulates earlier binding. Instead, the trio [Twi at 4-6h  $\rightarrow$  Twi at 2-4h  $\rightarrow$  Meso&SM] indicates that the effect of Twi binding at 4-6h on Meso&SM is likely mediated through Twi binding at 2-4h; these inferred relationships and such interpretation are consistent with Stojnic, Fu and Adryan (2012) (see Discussion for additional details).

We also ran order MCMC, partition MCMC, and scanBMA on this dataset to compare with baycn, using the edges confirmed and identified in Stojnic, Fu and Adryan (2012) as the ground truth. Similar to the previous section, an edge is considered present if the posterior probability for edge presence is at least 0.5. To summarize the results, we consider the inference correct if a method identifies the edge between a tissue and the binding profile of a TF at any time point (Figure 6C; Supplementary Table S22). Both baycn and scanBMA infer almost the same known tissue-TF relationships, whereas order and partition MCMC miss many of them, although for some edges order and partition MCMC inferred similar posterior probabilities to baycn (Supplementary Table S22).

**3. Discussion.** Here we present a novel approach to Bayesian inference of DAGs. We represent a graph by a list of edge states. A prior distribution can then be assigned to an edge, which makes it easy to experiment with different beliefs about the edge states (e.g., sparsity). We have developed an Metropolis-Hastings-like algorithm for approximate inference, which deals with directed cycles, accounts for Markov equivalence, and is applicable to diverse data types (continuous, discrete, and mixed). Our method can be used for causal inference when instrumental variables are available (with confounding variables appropriately accounted for). We have demonstrated through simulation studies that baycn is fast and can accurately estimate the edge probabilities in general, and that it performs as well as or better than current Bayesian methods in terms of precision, power, and mean squared error.

Our inference method takes a pseudo-likelihood approach to eliminate nuisance parameters and calculates the profile likelihood for a given graph. Although not a genuine likelihood, its impact on the inference of the graph structure is minor in large samples (Severini, 2000),



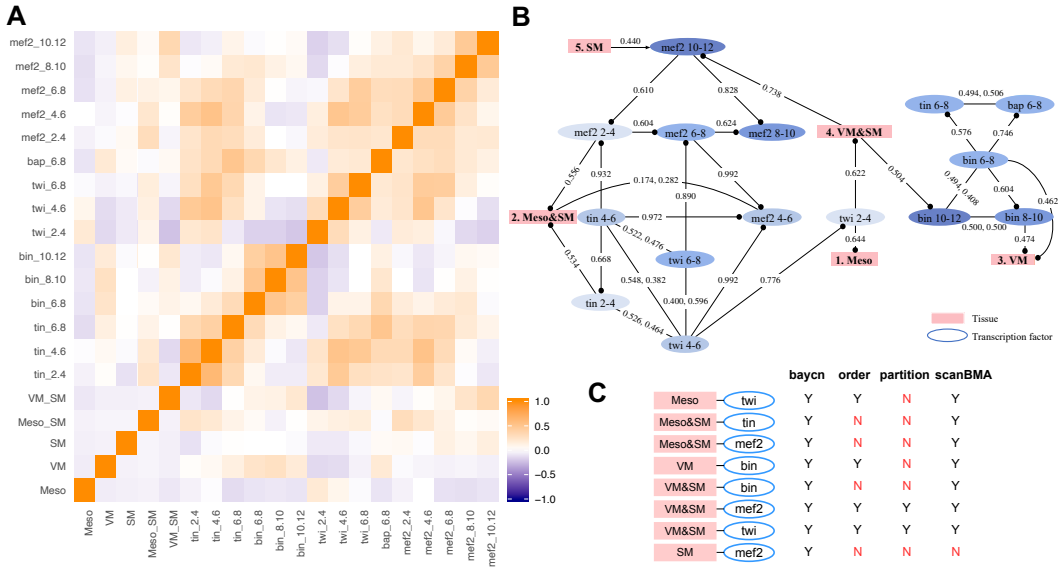


**Fig 6: Combinatorial binding of transcription factors (TFs) in five tissue types from the benchmark dataset on *Drosophila embryo* (Zinzen et al., 2009).** The TFs are: Twist (Twi), Tinman (Tin), Myocyte enhancing factor 2 (Mef2), Bagpipe (Bap), and Biniou (Bin). The tissue types are: mesoderm (Meso), mesoderm and somatic muscle (Meso&SM), visceral muscle (VM), visceral muscle and somatic muscle (VM&SM), and somatic muscle (SM). **(A)** The heatmap of Pearson correlations. **(B)** The network inferred by baycn. To avoid potential confusion with interpreting directed edges for these time series, we used a dot in place of an arrow. Except for bidirected edges, only the inferred direction with the corresponding posterior probability is shown. Shades of the TFs reflect the timing of the TF binding. **(C)** Known relationships between tissues and TFs with the corresponding presence/absence inference from each method. A relationship is considered to be present if a method infers at least one edge between any of the time points for a given TF and its associated tissue.

which is the case in our simulations and applications. Alternatively, the profile likelihood may be replaced by other pseudo-likelihoods such as a modified profile likelihood or a marginal likelihood (integrating out  $\theta$ ), although these pseudo-likelihoods each has its own computational challenges (Severini, 2000; Ventura and Racugno, 2016).

A caveat when interpreting the inferred network is that the direction of an edge indicates statistical dependence. With additional assumptions, the direction may also indicate the actual, causal mechanism. In the application of the eQTLs and their target genes, for example, we imposed the constraint that an edge between an eQTL and a gene always points to the latter. This is consistent with the biological principle that in general, DNA regulates RNA, but not the other way around. With this constraint, other directed edges may suggest regulatory relationships. For example, the subgraph [rs11305802  $\rightarrow$  PNP  $\rightarrow$  TMEM55B] in Figure 5 suggests that the eQTL rs11305803 likely regulates gene TMEM55B through gene PNP.

In the application to the transcription factor binding data, however, no suitable constraint was applied. As a result, the direction in Figure 6 should be interpreted carefully. Several directed edges, such as [Tin at 4-6h  $\rightarrow$  Mef2 at 2-4h], [Tin at 4-6h  $\rightarrow$  Tin at 2-4h], [Twi at 4-6h  $\rightarrow$  Twi at 2-4h], and [Mef2 at 10-12h  $\rightarrow$  Mef2 at 2-4h], and [Mef2 at 10-12h  $\rightarrow$  Mef2 at 8-10h], are inferred by at least two of the four Bayesian methods (Supplementary Table S22). However, these edges should not be interpreted as later binding regulating earlier binding. Instead, edge directions should be interpreted as conditional (in)dependence between nodes

and not biological regulation. For example, the subgraph [Tin at 4-6h  $\rightarrow$  Mef2 at 2-4h  $\rightarrow$  Meso&SM] indicates that the association between Tin at 4-6h and the tissue can be explained away by Mef2 at 2-4h; in other words, the formation of Meso&SM is more directly driven by Mef2 binding at 2-4h than by Tin binding at 4-6h. Similarly, in the subgraph [VM&SM  $\rightarrow$  Mef2 at 10-12h  $\rightarrow$  Mef2 at 8-10h], our method and the two MCMC methods all inferred the latter directed edge. This subgraph indicates that the association between Mef2 at 8-10h and VM&SM can be explained away by the later binding of Mef2 at 10-12h, meaning that the formation of VM&SM is more directly associated with Mef2 binding at a later time than at an earlier time.

The graphs we have analyzed here are still fairly small, and additional work is needed for baycn to handle much larger graphs of hundreds of nodes. However, our Bayesian method provides the much-needed ease to experiment with different beliefs about the edge states: we can increase or decrease the prior probability for a certain edge state. By comparing the posterior probabilities to the prior, the user can better assess how informative the data is and thus better interpret the inferred graph.

**Conflict of Interest Statement.** The authors declare that the research was conducted in the absence of any commercial or financial relationships that could be construed as a potential conflict of interest.

**Author Contributions.** EAM and AQF conceived the project. EAM developed the R package with the help of AQF and performed the simulations and data analyses. Both EAM and AQF contributed equally to writing the manuscript.

**Data Availability.** The method presented in this paper is implemented in the R package baycn available at <https://CRAN.R-project.org/package=baycn> or on GitHub at <https://github.com/evanamartin/baycn>.

The GEUVADIS data is publicly available at <https://www.ebi.ac.uk/biostudies/arrayexpress/studies/E-GEUV-3>. The Drosophila data is publicly available as Supplementary Table 8 of Zinzen et al. (2009). All simulated and real data (GEUVADIS and Drosophila data), as well as the code used for the analysis, is available on GitHub at [https://github.com/evanamartin/baycn\\_analysis\\_code](https://github.com/evanamartin/baycn_analysis_code). The real data is also included in the R package baycn.

Furthermore, we used the Gibbs and MC3 samplers in the R package structmcmc (<https://github.com/rjbgoudie/structmcmc>), the orderMCMC and partitionMCMC functions in the R package BiDAG (<https://cran.r-project.org/web/packages/BiDAG/index.html>), and the ScanBMA function in the R package networkBMA (<https://bioconductor.riken.jp/packages/3.2/bioc/html/networkBMA.html>).

**Acknowledgments.** The authors thank Robert J. B. Goudie for helping with the Gibbs sampler implemented in his structmcmc R package and Md. Bahadur Badsha for preparing the GEUVADIS data for analysis.

**Funding.** This work was supported by the NIH grants R00HG007368 and P20GM104420.

## SUPPLEMENTARY MATERIAL

The supplementary materials contain details of the algorithm, additional figures, and additional tables.

# Approximate Bayesian inference of directed acyclic graphs in biology with flexible priors on edge states

## Supplementary Materials

**Supplementary Notes.** Note: All of the references to equations and figures in Supplementary Notes refer to equations and figures in the Supplementary Materials file and not in the main text.

**4. Identifying and removing directed cycles.** In a directed cycle, one can follow the directed edges and return to the starting node (e.g.,  $T_1 \rightarrow T_2 \rightarrow T_3 \rightarrow T_1$ ). Directed cycles can have a higher likelihood than the true graph, a graph with directed edges but no cycles, and therefore should be removed during the sampling iterations when generating a proposal graph.

We have developed a “cycle finder” algorithm (Section 4.1) to find all directed cycles (including overlapping cycles, as well as multiple disjoint ones) in a graph, and a “cycle remover” algorithm (Section 4.2) to move out of directed cycles such that the proposed graph is free of directed cycles. It is plausible that when proposing a new graph, our sampling algorithm may propose a graph with one or more directed cycles, try to move out of these directed cycles only to generate a graph with different directed cycles. Therefore, our algorithm may need to repeatedly identify and remove directed cycles in one sampling iteration. However, since we focus on relatively small graphs in this paper, this scenario is rather unlikely.

### 4.1. Cycle finder algorithm.

1. Find the nodes that are connected to two or more nodes as a cycle contains at least three nodes and each node in a cycle has at least one incoming edge and one outgoing edge. To do so, we use the following steps:
  - i. Add the adjacency matrix to its transpose.
  - ii. Sum each row and delete rows (the row indices are preserved) with a sum less than 2.
  - iii. Apply the following rule to the adjacency matrix

$$\forall A_{j,k} = 1, \begin{cases} A_{j,k} = 0 & \text{if } k \notin J \\ A_{j,k} = 1 & \text{if } k \in J, \end{cases}$$

where  $J$  is the set of remaining row indices in the adjacency matrix.

- iv. Repeat steps ii and iii until  $\forall A_{j,k} = 1, k \in J$  or the reduced adjacency matrix has two or fewer rows.
2. Create a tree as deep as possible starting with the node (i.e., root node) whose index is in the first row of the reduced adjacency matrix. To do this we create a branch, which is a vector of node indices, for each of the nodes (i.e., child nodes) connected to the root. For each branch we add the index of the child node to the end of the vector, repeating the process of a child node becoming the parent node, until we add an index that has been added to the branch previously. If a parent node has two or more children a new branch is created for each child node.
3. Remove the nodes from the branches that do not belong to the cycle. In addition to the nodes that create a cycle a branch may also contain nodes outside the cycle. To remove these nodes, we start at the last node (i.e., the leaf) of the branches created in the previous step and work up the branch until we come to a node index that matches the leaf. Nodes above this node are then removed. For example, a branch may be (3, 4, 1, 6, 5, 2, 1) and the trimmed branch would be (1, 6, 5, 2, 1).

4. Convert the trimmed branches of a cycle into a vector of adjacency matrix coordinates by pairing up the adjacent nodes in each trimmed branch to produce a vector of edge coordinates. For example, if a trimmed branch is  $(1, 6, 5, 2, 1)$  then the adjacency matrix coordinates for the edges between the nodes in the cycle are  $((1, 6), (6, 5), (5, 2), (2, 1))$ .
5. Generate a vector of edge states from the vector of edge coordinates by considering each pair of coordinates and comparing the first number to the second number. If the first number is smaller than the second number the edge state is 0, indicating that the edge points from the node with a smaller index to the node with the larger index. If the first number is larger than the second number the edge state is 1, indicating that the edge points from the node with a larger index to the node with a smaller index. The coordinates vector from the example in Step 4 is  $((1, 6), (6, 5), (5, 2), (2, 1))$  and the edge states that form a directed cycle are  $(0, 1, 1, 1)$ .
6. Use the vector of edge coordinates from step 4 to create a vector of edge indices. For example, the edge indices for the coordinates  $((1, 6), (6, 5), (5, 2), (2, 1))$  are  $(2, 6, 5, 1)$ .
7. Define each cycle by the edges in the cycle and the states that form a cycle Using the vector of edge states (step 5) and the vector of edge indices (step 6). The cycle vector for the  $j$ th cycle is:

$$(8) \quad (S_1, S_2, \dots, S_m)$$

where  $m$  is the number of edges in the network and each  $S_k$  can take one of three values:

$$S_k = \begin{cases} 9 & \text{if this edge is not involved in the } j\text{th cycle} \\ 1 & \text{if edge } S_k \text{ is in state 1} \\ 0 & \text{if edge } S_k \text{ is in state 0.} \end{cases}$$

For example, Figure 7 shows a graph with two cycles nested within a larger cycle. If the edges are oriented as shown in the figure the cycle vector for the cycle involving edges  $(2, 3, 5, 6, 7)$  with states  $\mathbf{S} = (0, 1, 0, 0, 0)$  is

$$(9, 0, 1, 9, 0, 0, 0),$$

and the cycle vector for the cycle involving edges  $(1, 3, 4, 5, 6, 7)$  with states  $\mathbf{S} = (0, 1, 0, 0, 0, 0)$  is

$$(0, 9, 1, 0, 0, 0, 0).$$

Even though the cycles in the example above have four edges in common with the same edge direction for each of these edges, we are able to distinguish between the two cycles by comparing the cycle vectors elementwise.

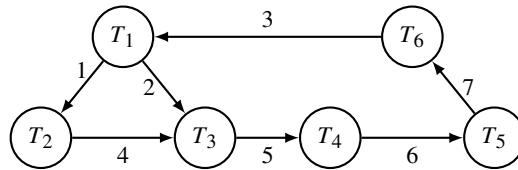


Fig 7: A graph with two directed cycles one cycle is made up of edges  $\{2, 5, 6, 7, 3\}$  and the other with edges  $\{1, 4, 5, 6, 7, 3\}$ . The two cycles have four edges in common.

#### 4.2. Cycle remover algorithm.

1. For the proposed graph create a cycle vector, from the proposed edge states, for each set of edges that could form a directed cycle. For example, if the graph shown in Figure 8b is the proposed graph then the cycle vector would be (0, 2, 1, 1).
2. For each set of edges that could form a directed cycle, compare the cycle vector of the proposed graph with the cycle vector of the directed cycles elementwise. For example, if the graph shown in Figure 8a is the true graph then the cycle vectors for the directed cycles would be (0, 1, 0, 1) and (1, 0, 1, 0). It is important to note that for each set of edges that could form a directed cycle there are two cycles: one with the edges oriented clockwise and another with the edges oriented counterclockwise. The cycle vector (created in the previous step) for the proposed graph is (0, 2, 1, 1) which does not match either of the directed cycle vectors. Therefore, the proposed graph does not have any directed cycles.
3. For each directed cycle, randomly select an edge and change it from its current state to a different state according to the prior probability of edge states.
4. Repeat steps 1 - 3 until there are no directed cycles in the graph.



Fig 8: The graphs used for an example of the cycle remover algorithm. a) The true graph and b) the proposed graph.

**5. Calculating the transition probability in our sampling algorithm.** Once a suitable proposal is generated, our sampling algorithm next calculates the acceptance probability for the proposed graph relative to the current one. Although the (repeated) removal of directed cycles enters the calculation of the transition probability between the current and proposed graph, the probabilities involving the cycles are in the end canceled in the calculation of the acceptance ratio. Let  $\mathbf{D}$  be a vector of indices of the edges that *differ* between the current graph  $\mathbf{S}$  and proposed graph  $\mathbf{S}'$  and  $\mathbf{C}$  be an integer vector where the element  $c_j$  indicates the number of edges that *can* change state for the edge denoted by  $d_j$  (see examples in Section 6). These two vectors have the same length, denoted by  $h$ . The probability of moving from  $\mathbf{S}$  to  $\mathbf{S}'$ , i.e.,  $\Pr(\mathbf{S} \rightarrow \mathbf{S}')$ , is the product of the probabilities of changes at individual edges in  $\mathbf{D}$ , and each of these probabilities further consists of two probabilities: the probability that an edge in the graph is chosen to change states, which is  $1/c_j$ , and the probability of edge  $d_j$  changing from its current state  $S_{d_j}$  to the state  $S'_{d_j}$ , denoted by  $\Pr(S_{d_j} \rightarrow S'_{d_j})$ . Therefore,

$$(9) \quad \Pr(\mathbf{S} \rightarrow \mathbf{S}') = \prod_{j=1}^h \frac{1}{c_j} \Pr(S_{d_j} \rightarrow S'_{d_j}) = \prod_{j=1}^h \frac{1}{c_j} \prod_{j=1}^h \Pr(S_{d_j} \rightarrow S'_{d_j}).$$

We prove that the transition probabilities do not depend on the path taken from the current graph to the proposed graph (the process of introducing and removing directed cycles) but only on the edges that have different states between the two graphs.

**THEOREM 2.** *When calculating the acceptance probability, the transition probabilities between the current graph  $\mathbf{S}$  and proposed graph  $\mathbf{S}'$ ,  $\Pr(\mathbf{S} \rightarrow \mathbf{S}')$  and  $\Pr(\mathbf{S}' \rightarrow \mathbf{S})$ , depend only on the edges whose states are different between the two graphs.*

**PROOF.** Recall that  $\mathbf{S}$  is a vector of edge states representing the current graph  $\mathcal{G}$  and  $\mathbf{S}'$  is a vector of edge states representing the proposal graph  $\mathcal{G}'$ . Let  $\mathbf{D}$  be a vector of indices of the edges that *differ* between the current graph  $\mathbf{S}$  and proposed graph  $\mathbf{S}'$  and  $\mathbf{C}$  be an integer vector where the element  $c_j$  represents the number of edges that *can* change state for the edge represented by  $d_j$ . These two vectors have the same length, denoted by  $h$ .

We will consider two cases: without and with potential directed cycles in the graph.

**CASE 1.** *Without potential directed cycles the probability of moving from the current graph to the proposed graph is*

$$\begin{aligned} \Pr(\mathbf{S} \rightarrow \mathbf{S}') &= \prod_{j=1}^h \frac{1}{c_j} \Pr(S_{d_j} \rightarrow S'_{d_j}) \\ (10) \qquad \qquad &= \prod_{j=1}^h \frac{1}{c_j} \prod_{j=1}^h \Pr(S_{d_j} \rightarrow S'_{d_j}). \end{aligned}$$

*We can use the same procedure of deriving the equation for moving back to the current graph from the proposed graph. Therefore, the probability can be broken down in the same way when moving backwards:*

$$(11) \qquad \Pr(\mathbf{S}' \rightarrow \mathbf{S}) = \prod_{j=1}^h \frac{1}{c_j} \prod_{j=1}^h \Pr(S'_{d_j} \rightarrow S_{d_j}).$$

*Since there are no potential directed cycles in the network the value  $c_j$  will always be  $m$  which is the number of edges in the network. Therefore,  $\prod_{j=1}^h \frac{1}{c_j} = \prod_{j=1}^h \frac{1}{m}$  whether going from  $\mathbf{S} \rightarrow \mathbf{S}'$  or  $\mathbf{S}' \rightarrow \mathbf{S}$  and will cancel when calculating the acceptance probability, leaving  $\prod_{j=1}^h \Pr(S_{d_j} \rightarrow S'_{d_j})$  and  $\prod_{j=1}^h \Pr(S'_{d_j} \rightarrow S_{d_j})$ .*

**CASE 2.** *With potential directed cycles there can be multiple paths when moving from the current graph to the proposed graph. Let  $\mathbf{C}^k$  be a vector where each  $c_j^k$  is the number of edges that can change state in path  $k$  when moving from  $\mathbf{S}$  to  $\mathbf{S}'$  and  $\mathbf{C}^{k'}$  be a vector where each  $c_j^{k'}$  is the number of edges that can change state in path  $k$  when moving from  $\mathbf{S}'$  to  $\mathbf{S}$ . Using Equation (10) the transition probability of moving from the current graph to the proposed graph when there are multiple paths becomes*

$$(12) \qquad \Pr(\mathbf{S} \rightarrow \mathbf{S}') = \sum_{k=1}^K \prod_{j=1}^h \frac{1}{c_j^k} \prod_{j=1}^h \Pr(S_{d_j} \rightarrow S'_{d_j}) = \prod_{j=1}^h \Pr(S_{d_j} \rightarrow S'_{d_j}) \sum_{k=1}^K \prod_{j=1}^h \frac{1}{c_j^k}.$$

*Similarly, the transition probability when there are multiple paths of moving back to the current graph from the proposed graph is*

$$(13) \qquad \Pr(\mathbf{S}' \rightarrow \mathbf{S}) = \sum_{k=1}^K \prod_{j=1}^h \frac{1}{c_j^{k'}} \prod_{j=1}^h \Pr(S'_{d_j} \rightarrow S_{d_j}) = \prod_{j=1}^h \Pr(S'_{d_j} \rightarrow S_{d_j}) \sum_{k=1}^K \prod_{j=1}^h \frac{1}{c_j^{k'}}.$$

*In Equations (12) and (13) the summation over  $K$  represents the different paths (Section 6) to get from one graph to another and the last equality holds because the edges that are different between  $\mathbf{S}$  and  $\mathbf{S}'$  do not depend on the path  $k$ .*

For each path  $k$

$$(14) \quad \mathbf{C}^k = (c_1^k, c_2^k, c_3^k, \dots, c_h^k)$$

$$(15) \quad = \underbrace{(c_1^k, c_2^k, \dots, c_j^k)}_{\text{create cycle(s)}} \underbrace{(c_{j+1}^k, \dots, c_h^k)}_{\text{remove cycle(s)}}$$

$$(16) \quad = \underbrace{(m, \dots, m)}_j, c_{j+1}^k, \dots, c_h^k.$$

The first  $j$  elements can create one or more directed cycles. The remaining  $h - j$  elements then remove the cycle(s) that were introduced in the network and their values are equal to the number of edges that make up the directed cycle that is being removed. The cycles that are created and removed in any path  $k$  from  $\mathbf{S}$  to  $\mathbf{S}'$  can also be created and removed when moving from  $\mathbf{S}'$  to  $\mathbf{S}$ . Therefore, the equations for moving from the proposed graph to the current graph will be the same as Equations (14) - (16) except for the ' symbol indicating that we are moving backwards:

$$(17) \quad \mathbf{C}^{k'} = (c_1^{k'}, c_2^{k'}, c_3^{k'}, \dots, c_h^{k'})$$

$$(18) \quad = \underbrace{(c_1^{k'}, c_2^{k'}, \dots, c_j^{k'})}_{\text{create cycle(s)}} \underbrace{(c_{j+1}^{k'}, \dots, c_h^{k'})}_{\text{remove cycle(s)}}$$

$$(19) \quad = \underbrace{(m, \dots, m)}_j, c_{j+1}^{k'}, \dots, c_h^{k'},$$

and

$$(20) \quad \sum_{k=1}^K \prod_{j=1}^h \frac{1}{c_j^k} = \sum_{k=1}^K \prod_{j=1}^h \frac{1}{c_j^{k'}}.$$

The terms in Equation (20) will cancel when calculating the acceptance probability and we will be left with  $\prod_{j=1}^h \Pr(S_{d_j} \rightarrow S'_{d_j})$  and  $\prod_{j=1}^h \Pr(S'_{d_j} \rightarrow S_{d_j})$ .

■

See Section 6 for examples.

## 6. Examples of Theorem 1.

*Example 1 – one directed cycle.* Consider the current graph in Figure 9a with states  $\mathbf{S} = (0, 0, 0, 1, 1)$  and the proposed graph in Figure 9c with states  $\mathbf{S}' = (0, 1, 2, 1, 1)$ . Edges #2 and #3 have different states between  $\mathbf{S}$  and  $\mathbf{S}'$  therefore  $\mathbf{D} = 2, 3$ . There are two different paths to move from  $\mathbf{S}$  to  $\mathbf{S}'$ . In path 1 there are two steps: i) edge #2 changes direction which creates a directed cycle between nodes  $T_1$ ,  $T_2$ , and  $T_3$  (Figure 9b) and ii) the directed cycle is removed by edge #3 changing from state 0 to 2. In path 2 edges #2 and #3 change states in one step. If the prior on edge states is  $p_0 = 0.05$ ,  $p_1 = 0.05$  and  $p_2 = 0.9$  then the probabilities for the two paths are

$$\text{path 1: } \Pr(S_{d_2} \rightarrow S'_{d_2}) = \frac{0.05}{0.95}, \Pr(S_{d_3} \rightarrow S'_{d_3}) = \frac{0.9}{0.95}, \mathbf{C}^1 = 5, 3$$

and

$$\text{path 2: } \Pr(S_{d_2} \rightarrow S'_{d_2}) = \frac{0.05}{0.95}, \Pr(S_{d_3} \rightarrow S'_{d_3}) = \frac{0.9}{0.95}, \mathbf{C}^2 = 5, 5.$$



Combining the probabilities from each path we obtain the transition probability of moving to the proposed graph:

$$(21) \quad \Pr(\mathbf{S} \rightarrow \mathbf{S}') = \frac{1}{5} \frac{1}{3} \frac{0.05}{0.95} \frac{0.9}{0.95} + \frac{1}{5} \frac{1}{5} \frac{0.05}{0.95} \frac{0.9}{0.95} = \left( \frac{1}{5} \frac{1}{3} + \left( \frac{1}{5} \right)^2 \right) \frac{0.05}{0.95} \frac{0.9}{0.95}.$$

Any directed cycle created when moving from  $\mathbf{S}$  to  $\mathbf{S}'$  needs to be created when moving from  $\mathbf{S}'$  to  $\mathbf{S}$ . Therefore, when moving from  $\mathbf{S}'$  to  $\mathbf{S}$  there are also two paths. Path 1 is made up of two steps: i) edge #3 changes from state 2 to 0 creating a cycle between nodes  $T_1$ ,  $T_2$ , and  $T_3$  and ii) the cycle is removed by changing edge #2 from state 1 to 0. For path 2 edges #2 and #3 both change states in one step. The probabilities for the paths are

$$\text{path 1: } \Pr(S'_{d_2} \rightarrow S_{d_2}) = \frac{0.05}{0.95}, \Pr(S'_{d_3} \rightarrow S_{d_3}) = \frac{0.05}{0.1}, \mathbf{C}^{1'} = 5, 3$$

and

$$\text{path 2: } \Pr(S'_{d_2} \rightarrow S_{d_2}) = \frac{0.05}{0.95}, \Pr(S'_{d_3} \rightarrow S_{d_3}) = \frac{0.05}{0.1}, \mathbf{C}^{2'} = 5, 5.$$

The transition probability of moving back to the current graph is

$$(22) \quad \Pr(\mathbf{S}' \rightarrow \mathbf{S}) = \frac{1}{5} \frac{1}{3} \frac{0.05}{0.95} \frac{0.05}{0.1} + \frac{1}{5} \frac{1}{5} \frac{0.05}{0.95} \frac{0.05}{0.1} = \left( \frac{1}{5} \frac{1}{3} + \left( \frac{1}{5} \right)^2 \right) \frac{0.05}{0.95} \frac{0.05}{0.1}.$$

The term  $\frac{1}{5} \frac{1}{3} + \left( \frac{1}{5} \right)^2$  in Equations (21) and (22) cancels out when calculating the acceptance probability,  $\alpha$ , and we are left with the probability of moving between the states that differ between the current graph (Figure 9a) and the proposed graph (Figure 9c). More generally, we can apply the same procedure to traverse the paths between any two graphs.

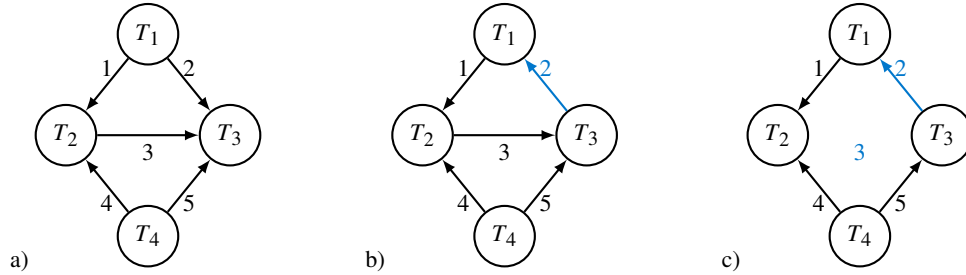


Fig 9: The graphs for example 1. a) The current graph. b) An intermediate graph between the current graph and the proposed graph where a directed cycle has been introduced into the network. c) The proposed graph.

*Example 2 – multiple directed cycles.* We show a second more complex example below. If we start with the graph in Figure 10a with states  $\mathbf{S} = (0, 0, 0, 1, 1)$  and the proposed graph in Figure 10d with states  $\mathbf{S}' = (2, 1, 1, 1, 0)$  there are four edges with different states between the two graphs and  $\mathbf{D} = 1, 2, 3, 5$ . There are three different paths to move from  $\mathbf{S}$  to  $\mathbf{S}'$ . The steps in path 1 are: i) edges #2 and #5 change directions creating two directed cycles, the first cycle is between nodes  $T_1$ ,  $T_2$ , and  $T_3$  and the second cycle is between nodes  $T_2$ ,  $T_3$ , and  $T_4$  (Figure 10b), ii) edge #1 changes from state 0 to 2 removing the first cycle (Figure 10c), and iii) edge #3 changes direction which removes the second cycle (Figure 10d). The steps in path 2 are: i) edges #1, #2, and #5 all change states creating one directed cycle between nodes  $T_2$ ,  $T_3$ , and  $T_4$  (Figure 10c) and ii) edge #3 changes direction removing the cycle. In path 3 edges #1, #2, #3, and #5 all change states in one step. If the prior on edge states is

$p_0 = 0.05$ ,  $p_1 = 0.05$ , and  $p_2 = 0.9$  then the probabilities for the three paths are:

path 1:

$$\begin{aligned}\Pr(S_{d_1} \rightarrow S'_{d_1}) &= \frac{0.9}{0.95}, \Pr(S_{d_2} \rightarrow S'_{d_2}) = \frac{0.05}{0.95}, \\ \Pr(S_{d_3} \rightarrow S'_{d_3}) &= \frac{0.05}{0.95}, \Pr(S_{d_5} \rightarrow S'_{d_5}) = \frac{0.05}{0.95}, \\ \mathbf{C}^1 &= 5, 5, 3, 3,\end{aligned}$$

path 2:

$$\begin{aligned}\Pr(S_{d_1} \rightarrow S'_{d_1}) &= \frac{0.9}{0.95}, \Pr(S_{d_2} \rightarrow S'_{d_2}) = \frac{0.05}{0.95}, \\ \Pr(S_{d_3} \rightarrow S'_{d_3}) &= \frac{0.05}{0.95}, \Pr(S_{d_5} \rightarrow S'_{d_5}) = \frac{0.05}{0.95}, \\ \mathbf{C}^2 &= 5, 5, 5, 3,\end{aligned}$$

and path 3:

$$\begin{aligned}\Pr(S_{d_1} \rightarrow S'_{d_1}) &= \frac{0.9}{0.95}, \Pr(S_{d_2} \rightarrow S'_{d_2}) = \frac{0.05}{0.95}, \\ \Pr(S_{d_3} \rightarrow S'_{d_3}) &= \frac{0.05}{0.95}, \Pr(S_{d_5} \rightarrow S'_{d_5}) = \frac{0.05}{0.95}, \\ \mathbf{C}^3 &= 5, 5, 5, 5.\end{aligned}$$

Therefore, the transition probability of moving to the proposed graph is

$$\begin{aligned}\Pr(\mathbf{S} \rightarrow \mathbf{S}') &= \frac{1}{5} \frac{1}{5} \frac{1}{3} \frac{1}{3} \frac{0.9}{0.95} \frac{0.05}{0.95} \frac{0.05}{0.95} \frac{0.05}{0.95} + \frac{1}{5} \frac{1}{5} \frac{1}{5} \frac{1}{3} \frac{0.9}{0.95} \frac{0.05}{0.95} \frac{0.05}{0.95} \frac{0.05}{0.95} \\ &+ \frac{1}{5} \frac{1}{5} \frac{1}{5} \frac{1}{5} \frac{0.9}{0.95} \frac{0.05}{0.95} \frac{0.05}{0.95} \frac{0.05}{0.95} \\ (23) \quad &= \left( \left( \frac{1}{5} \right)^2 \left( \frac{1}{3} \right)^2 + \left( \frac{1}{5} \right)^3 \frac{1}{3} + \left( \frac{1}{5} \right)^4 \right) \frac{0.9}{0.95} \frac{0.05}{0.95} \frac{0.05}{0.95} \frac{0.05}{0.95}.\end{aligned}$$

As in example 1 any directed cycle that is created when moving from  $\mathbf{S}$  to  $\mathbf{S}'$  needs to also be created when moving from  $\mathbf{S}'$  to  $\mathbf{S}$ . There are also three different paths to move back to  $\mathbf{S}$  from  $\mathbf{S}'$ . In path 1 the steps are: i) edges #1 and #3 change states creating two directed cycles the first cycle is between nodes  $T_1$ ,  $T_2$ , and  $T_3$  and the second cycle is between nodes  $T_2$ ,  $T_3$ , and  $T_4$ , ii) edge #2 changes direction removing the first cycle, and iii) edge #5 changes direction removing the second directed cycle. Path 2 has two steps i) edges #1, #2 and #3 all change state creating a directed cycle between nodes  $T_2$ ,  $T_3$ , and  $T_4$  and ii) edge #5 changes direction removing the cycle. In path 3 there is only one step where edges #1, #2, #3, and #5 all change states. The probabilities for these paths are

path 1:

$$\begin{aligned}\Pr(S'_{d_1} \rightarrow S_{d_1}) &= \frac{0.05}{0.1}, \Pr(S'_{d_2} \rightarrow S_{d_2}) = \frac{0.05}{0.95}, \\ \Pr(S'_{d_3} \rightarrow S_{d_3}) &= \frac{0.05}{0.95}, \Pr(S'_{d_5} \rightarrow S_{d_5}) = \frac{0.05}{0.95}, \\ \mathbf{C}^{1'} &= 5, 5, 3, 3,\end{aligned}$$

path 2:

$$\begin{aligned}\Pr(S'_{d_1} \rightarrow S_{d_1}) &= \frac{0.05}{0.1}, \Pr(S'_{d_2} \rightarrow S_{d_2}) = \frac{0.05}{0.95}, \\ \Pr(S'_{d_3} \rightarrow S_{d_3}) &= \frac{0.05}{0.95}, \Pr(S'_{d_5} \rightarrow S_{d_5}) = \frac{0.05}{0.95}, \\ \mathbf{C}^{2'} &= 5, 5, 5, 3,\end{aligned}$$

and path 3:

$$\begin{aligned}\Pr(S'_{d_1} \rightarrow S_{d_1}) &= \frac{0.05}{0.1}, \Pr(S'_{d_2} \rightarrow S_{d_2}) = \frac{0.05}{0.95}, \\ \Pr(S'_{d_3} \rightarrow S_{d_3}) &= \frac{0.05}{0.95}, \Pr(S'_{d_5} \rightarrow S_{d_5}) = \frac{0.05}{0.95}, \\ \mathbf{C}^{3'} &= 5, 5, 5, 5.\end{aligned}$$

Therefore, the transition probability of moving back to the current graph is

$$\begin{aligned}\Pr(\mathbf{S}' \rightarrow \mathbf{S}) &= \frac{1}{5} \frac{1}{5} \frac{1}{3} \frac{1}{3} \frac{0.05}{0.1} \frac{0.05}{0.95} \frac{0.05}{0.95} \frac{0.05}{0.95} + \frac{1}{5} \frac{1}{5} \frac{1}{5} \frac{1}{3} \frac{0.05}{0.1} \frac{0.05}{0.95} \frac{0.05}{0.95} \frac{0.05}{0.95} \\ &+ \frac{1}{5} \frac{1}{5} \frac{1}{5} \frac{1}{5} \frac{0.05}{0.1} \frac{0.05}{0.95} \frac{0.05}{0.95} \frac{0.05}{0.95} \\ (24) \quad &= \left( \left( \frac{1}{5} \right)^2 \left( \frac{1}{3} \right)^2 + \left( \frac{1}{5} \right)^3 \frac{1}{3} + \left( \frac{1}{5} \right)^4 \right) \frac{0.05}{0.1} \frac{0.05}{0.95} \frac{0.05}{0.95} \frac{0.05}{0.95}.\end{aligned}$$

The term  $\left( \frac{1}{5} \right)^2 \left( \frac{1}{3} \right)^2 + \left( \frac{1}{5} \right)^3 \frac{1}{3} + \left( \frac{1}{5} \right)^4$  in Equations (23) and (24) cancels out when calculating the acceptance probability,  $\alpha$ , and we are left with the probability of moving between the states that differ between the current graph (Figure 10a) and the proposed graph (Figure 10d). More generally, we can apply the same procedure to traverse the paths between any two graphs.

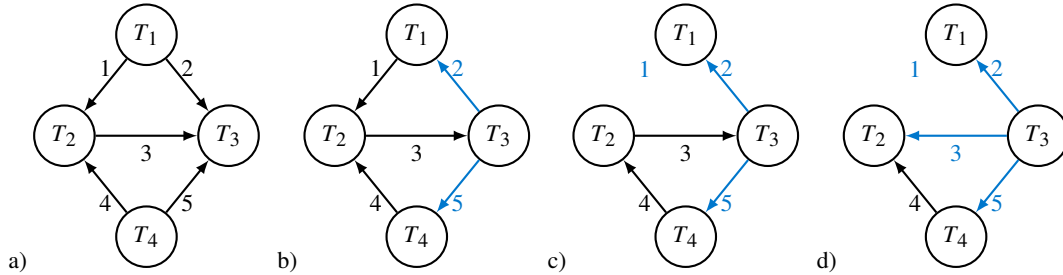


Fig 10: a) The current graph. b) An intermediate graph between the current graph and the proposed graph where two directed cycles have been introduced into the graph. c) An intermediate graph where one of the directed cycles has been removed. d) The proposed graph.

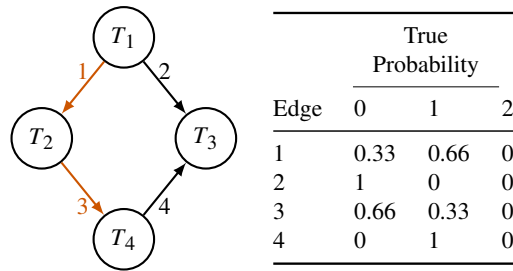


Fig S1: The true graph and probabilities for each edge in topology GN4. The edges in orange can change direction while remaining in the Markov equivalence class of the true graph – as long as another v-structure is not created.

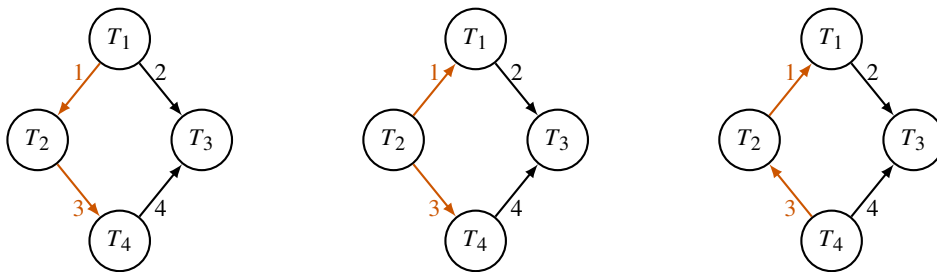


Fig S2: The Markov equivalence class of topology GN4. The edges in orange show all possible combinations of edge directions of the Markov equivalence class. Edge 1 is oriented  $T_1 \rightarrow T_2$  in one of the three graphs, giving a proportion of 0.33 for edge state 0. Edge 2 is oriented  $T_2 \rightarrow T_4$  in two of the three graphs, giving a proportion of 0.66 for state 0.

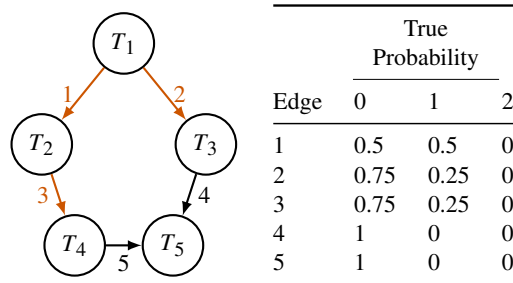


Fig S3: The true graph and probabilities for each edge in topology GN5. The edges in orange can change direction while remaining in the Markov equivalence class of the true graph – as long as another v-structure is not created.

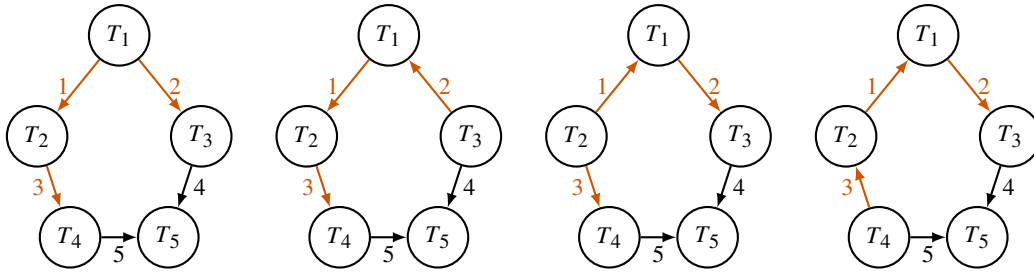


Fig S4: The Markov equivalence class of topology GN5. The edges in orange show all possible combinations of edge directions of the Markov equivalence class. In two of the four graphs edge 1 is oriented  $T_1 \rightarrow T_2$ , giving a proportion of 0.5 for edge state 0. In three of the four graphs edge 2 is oriented  $T_1 \rightarrow T_3$ , giving a proportion of 0.75 for edge state 0. Similarly, edge 3 is oriented  $T_2 \rightarrow T_4$  in three of the four graphs, giving a proportion of 0.75 for edge state 0.

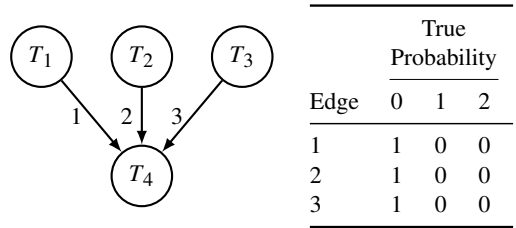


Fig S5: The true graph and probabilities for each edge in the multi-parent topology.

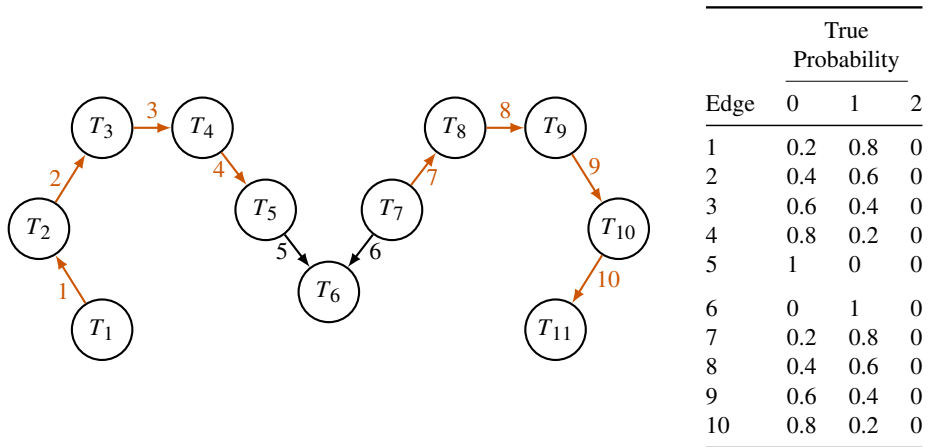


Fig S6: The true graph and probabilities for each edge in topology GN11. The edges in orange can change direction while remaining in the Markov equivalence class of the true graph – as long as another v-structure is not created.

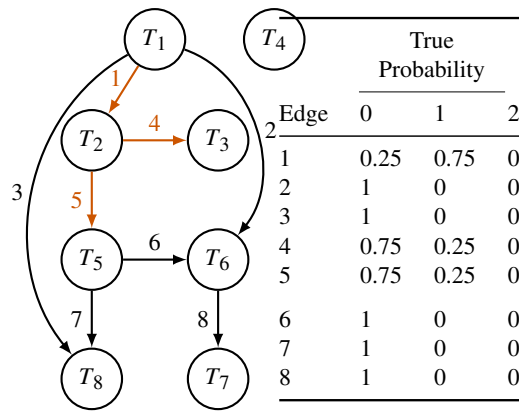


Fig S7: The true graph and probabilities for each edge in topology GN8. The edges in orange can change direction while remaining in the Markov equivalence class of the true graph – as long as another v-structure is not created.

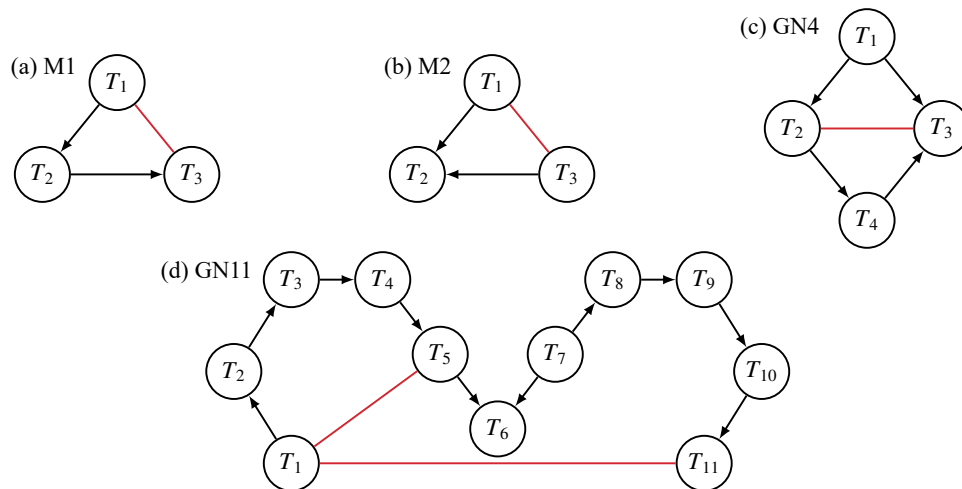


Fig S8: The black edges (true edges) were used to simulate the data and the red edges (false edges) were added to the true adjacency matrix as input to baycn.

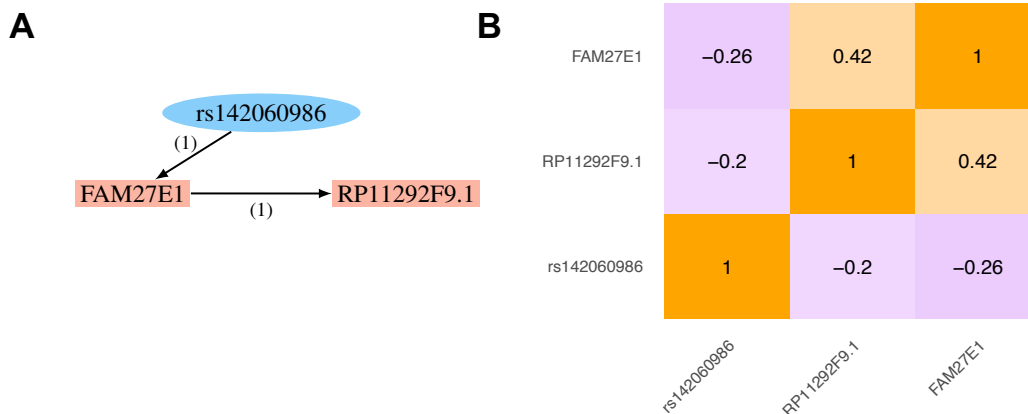


Fig S9: Inference of the GEUVADIS eQTL-gene set Q20, which does not have associated PCs. (A) Inferred graph with posterior probabilities. Numbers in parenthesis next to the edges indicate the posterior probability for the direction shown. (B) Correlation heatmap.

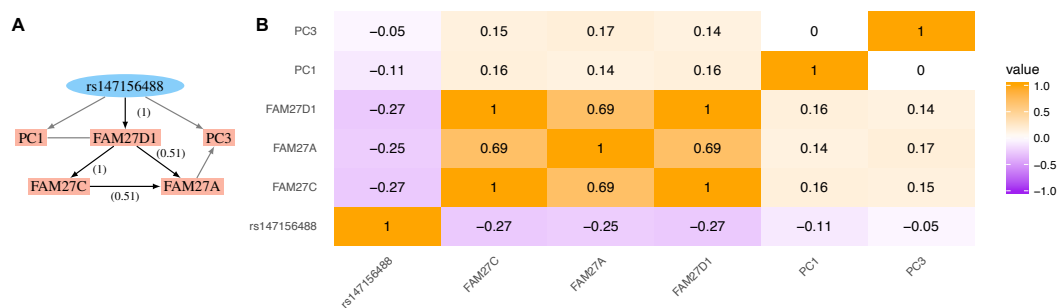


Fig S10: Inference of the GEUVADIS eQTL-gene set Q21 with associated PCs. (A) Inferred graph with posterior probabilities. Numbers in parenthesis next to the edges indicate the posterior probability for the direction shown. (B) Correlation heatmap.

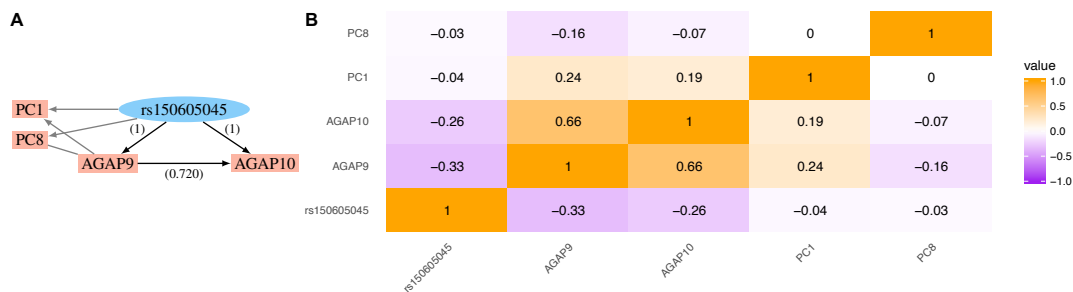


Fig S11: Inference of the GEUVADIS eQTL-gene set Q23 with associated PCs. (A) Inferred graph with posterior probabilities. Numbers in parenthesis next to the edges indicate the posterior probability for the direction shown. (B) Correlation heatmap.



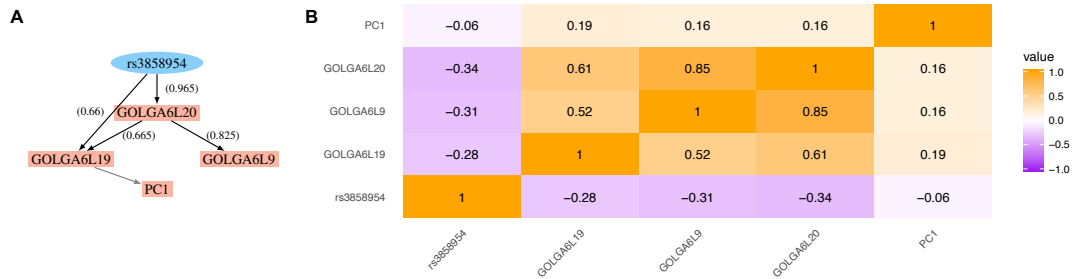


Fig S12: Inference of the GEUVADIS eQTL-gene set Q237 with associated PCs. (A) Inferred graph with posterior probabilities. Numbers in parenthesis next to the edges indicate the posterior probability for the direction shown. (B) Correlation heatmap.

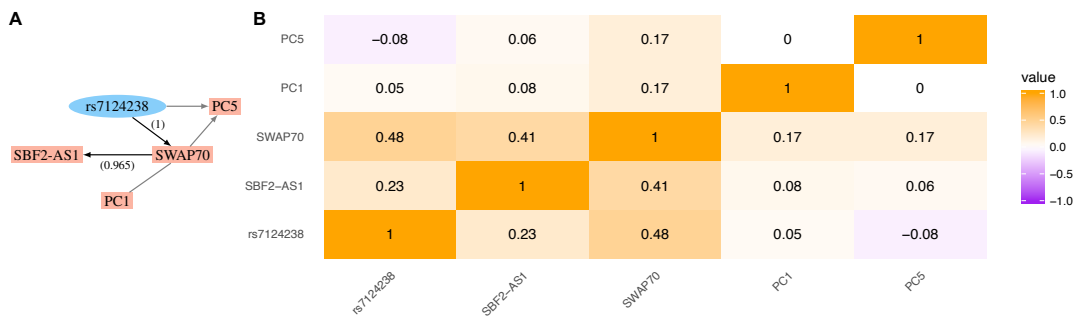


Fig S13: Inference of the GEUVADIS eQTL-gene set Q50 with associated PCs. (A) Inferred graph with posterior probabilities. Numbers in parenthesis next to the edges indicate the posterior probability for the direction shown. (B) Correlation heatmap.

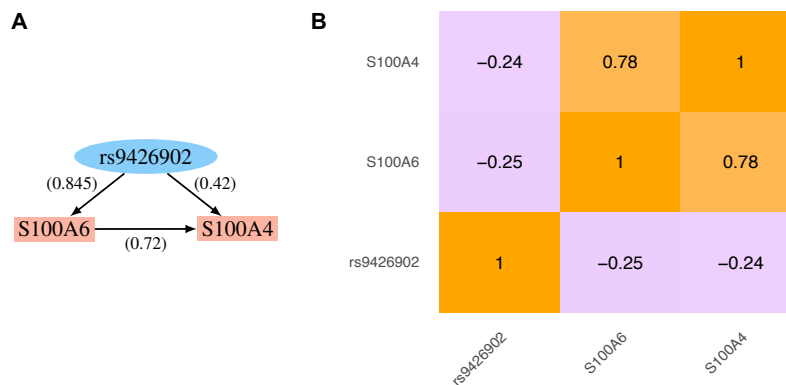


Fig S14: Inference of the GEUVADIS eQTL-gene set Q62, which does not have associated PCs. (A) Inferred graph with posterior probabilities. Numbers in parenthesis next to the edges indicate the posterior probability for the direction shown. (B) Correlation heatmap.

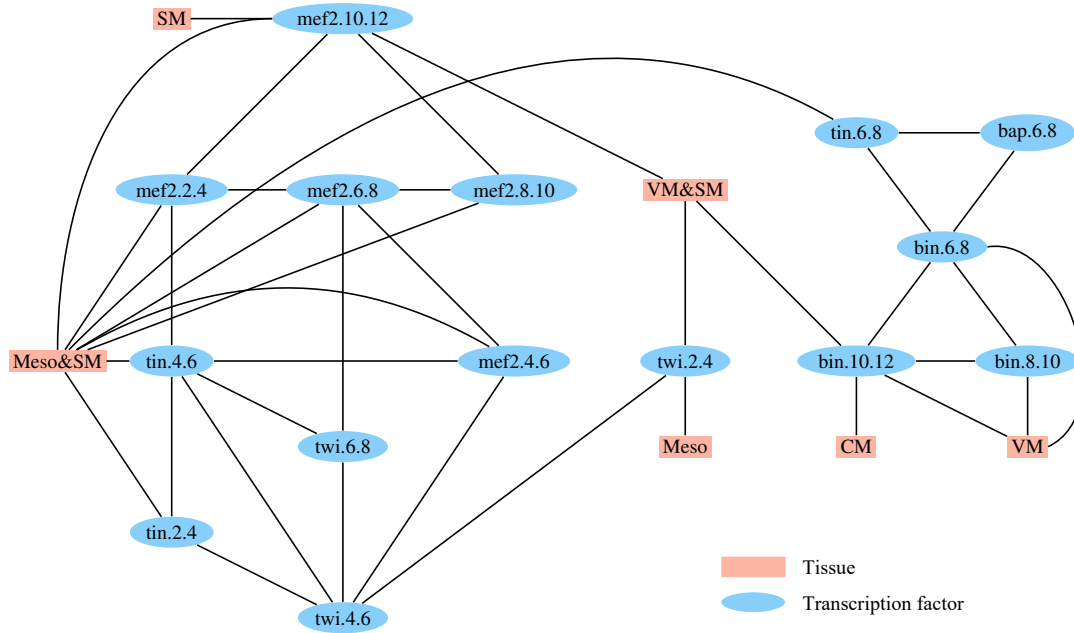


Fig S15: Graph used as the input to baycn for the Drosophila data. We first used the graph output by MRPC then added additional edges between Meso&SM and the transcription factors Mef2 and Tin and between VM and the transcription factor Bin.

### Supplementary Figures.

TABLE S1

Performance of baycn on all the graphs used in simulation studies. Features of the graphs in Figure 1 in the main text, such as the number of edges and v-structures, are listed. The mean and standard deviation of  $MSE_1$  (on three states of each edge), sample size  $N$ , and signal strength  $\beta$  are also listed. For each simulation scenario we generated 25 independent data sets and ran baycn once on each data set.

Topology	# edges	# v-structures	$N$	$MSE_1$					
				$\beta = 0.2$		$\beta = 0.5$		$\beta = 1$	
				mean	sd	mean	sd	mean	sd
M1	2	0	100	0.1796	0.0949	0.0127	0.0353	0.0011	0.0016
			200	0.0734	0.074	0.0014	0.0015	0.0012	0.0013
			600	0.0237	0.0326	0.001	0.0009	0.0008	0.0007
M2	2	1	100	0.3384	0.1081	0.0909	0.0919	0	0
			200	0.2688	0.0881	0.0597	0.082	0	0
			600	0.1323	0.0735	0	0	0	0
GN4	4	1	100	0.2731	0.0711	0.0674	0.0417	0.01	0.0276
			200	0.167	0.0554	0.0755	0.0639	0.0046	0.0142
			600	0.0839	0.0259	0.0503	0.0602	0.0069	0.0182
GN5	5	1	100	0.2687	0.0785	0.0396	0.0465	0.0022	0.0023
			200	0.1562	0.049	0.0171	0.0235	0.002	0.0031
			600	0.0684	0.0338	0.0114	0.0483	0.002	0.0024
Mult-parent	3	3	100	0.3361	0.0961	0.0486	0.0698	0	0
			200	0.237	0.0812	0.0032	0.0135	0	0
			600	0.1418	0.0625	0	0.0002	0	0
GN11	10	1	100	0.2266	0.0513	0.0353	0.0225	0.0042	0.0031
			200	0.139	0.0431	0.0121	0.0162	0.0066	0.0041
			600	0.0613	0.0197	0.0047	0.0043	0.0046	0.0039
GN8	8	2	100	0.2959	0.1517	0.0667	0.0666	0.0247	0.0526
			200	0.197	0.144	0.0692	0.0962	0.0186	0.0486
			600	0.1147	0.1073	0.0556	0.0858	0.0109	0.0467

TABLE S2

The mean and standard deviation of the edge-wise MSE for each edge in topology M1. We used the data sets previously simulated for M1 and included one false edge with the true edges in the input to baycn. We ran baycn with three different priors on edge states for each data set. The rows in red represent false edges.

		eMSE: Topology M1					
$N$	Edge	Prior 1		Prior 2		Prior 3	
		mean	sd	mean	sd	mean	sd
100	1	0.0109	0.006	0.0078	0.0047	0.002	0.0026
	2	0.2853	0.0568	0.1859	0.0618	0.0131	0.0139
	3	0.0107	0.0061	0.0091	0.0059	0.0014	0.0015
200	1	0.0116	0.0067	0.0075	0.005	0.002	0.0027
	2	0.2861	0.0816	0.1953	0.0992	0.03	0.0614
	3	0.0109	0.0063	0.0094	0.0046	0.0019	0.0025
600	1	0.0127	0.0062	0.008	0.0056	0.0008	0.001
	2	0.2665	0.038	0.1593	0.052	0.0095	0.0068
	3	0.0139	0.0085	0.0062	0.004	0.0016	0.0021

TABLE S3

The mean and standard deviation of the edge-wise MSE for each edge in topology M2. We used the data sets previously simulated for M2 and included one false edge with the true edges in the input to baycn. We ran baycn with three different priors on edge states for each data set. The rows in red represent false edges.

		eMSE: Topology M2					
N	Edge	Prior 1		Prior 2		Prior 3	
		mean	sd	mean	sd	mean	sd
100	1	0.1366	0.0269	0.1197	0.0199	0.0224	0.026
	2	0.4035	0.0368	0.3285	0.0548	0.0656	0.0666
	3	0.1461	0.025	0.1241	0.0226	0.0232	0.028
200	1	0.1329	0.0262	0.1215	0.0222	0.0297	0.0354
	2	0.4111	0.0373	0.3474	0.0612	0.0863	0.0975
	3	0.1391	0.0227	0.1209	0.0245	0.0317	0.0396
600	1	0.1369	0.0207	0.1183	0.0221	0.0236	0.0164
	2	0.4062	0.0347	0.3362	0.0459	0.0647	0.0377
	3	0.1378	0.028	0.1186	0.0223	0.0224	0.0149

TABLE S4

The mean and standard deviation of the edge-wise MSE for each edge in topology GN4. We used the data sets previously simulated for GN4 and included one false edge with the true edges in the input to baycn. We ran baycn with three different priors on edge states for each data set. The rows in red represent false edges.

		eMSE: Topology GN4					
N	Edge	Prior 1		Prior 2		Prior 3	
		mean	sd	mean	sd	mean	sd
100	1	0.0101	0.0182	0.011	0.0165	0.0418	0.0797
	2	0.011	0.0204	0.0098	0.0192	0.0431	0.0821
	3	0.2235	0.1185	0.1368	0.1257	0.0301	0.1031
	4	0.0085	0.0148	0.0078	0.0132	0.0462	0.0817
	5	0.0087	0.0162	0.0107	0.0203	0.0459	0.0888
200	1	0.0012	0.0023	0.0019	0.0036	0.0152	0.0414
	2	0.0004	0.0013	0.0012	0.004	0.0156	0.0462
	3	0.2154	0.079	0.1139	0.0669	0.005	0.0083
	4	0.0013	0.002	0.0023	0.0045	0.0181	0.0432
	5	0.0003	0.001	0.0013	0.0043	0.012	0.0317
600	1	0.0008	0.0015	0.0009	0.001	0.0103	0.0387
	2	0	0	0	0	0.0102	0.0402
	3	0.2534	0.1019	0.1544	0.1028	0.0092	0.0201
	4	0.0007	0.0012	0.0012	0.0015	0.011	0.038
	5	0	0	0	0	0.0112	0.0503

TABLE S5

The mean and standard deviation of the edge-wise MSE for each edge in topology GN11. We used the data sets previously simulated for GN11 and included two false edges with the true edges in the input to baycn. We ran baycn with three different priors on edge states for each data set. The rows in red represent false edges.

		eMSE: Topology GN11					
$N$	Edge	Prior 1		Prior 2		Prior 3	
		mean	sd	mean	sd	mean	sd
100	1	0.0023	0.0035	0.003	0.0038	0.0046	0.006
	2	0.2976	0.1311	0.2084	0.1464	0.0386	0.1027
	3	0.2931	0.0658	0.2039	0.0851	0.0168	0.0239
	4	0.0018	0.0028	0.0035	0.0033	0.009	0.0104
	5	0.0029	0.0046	0.0037	0.0048	0.0087	0.0116
	6	0.0045	0.007	0.0043	0.0064	0.0038	0.0044
	7	0	0	0	0	0	0
	8	0	0	0	0	0	0
	9	0.0009	0.0011	0.0014	0.0023	0.0037	0.005
	10	0.0018	0.002	0.002	0.0025	0.0107	0.0153
	11	0.002	0.0019	0.0024	0.0029	0.0097	0.0132
	12	0.0016	0.0018	0.0016	0.0026	0.0044	0.0057
200	1	0.0048	0.0046	0.0033	0.0042	0.0029	0.0036
	2	0.286	0.1233	0.1938	0.1334	0.0338	0.0753
	3	0.3161	0.0676	0.2138	0.0676	0.0188	0.0152
	4	0.0032	0.0052	0.0028	0.0038	0.0076	0.0092
	5	0.0026	0.0043	0.0029	0.006	0.0069	0.0085
	6	0.0041	0.0056	0.0032	0.0056	0.0039	0.0052
	7	0	0	0	0	0	0
	8	0	0	0	0	0	0
	9	0.0006	0.0009	0.0004	0.0005	0.008	0.0137
	10	0.0013	0.0016	0.0007	0.0013	0.0115	0.0148
	11	0.0018	0.0021	0.0014	0.002	0.0093	0.0112
	12	0.0021	0.0025	0.0012	0.0018	0.0038	0.0041
600	1	0.0069	0.0069	0.0052	0.0058	0.0048	0.0056
	2	0.2735	0.0938	0.1783	0.0949	0.0147	0.0231
	3	0.3436	0.1118	0.2446	0.129	0.0557	0.1172
	4	0.0049	0.0062	0.0028	0.003	0.0108	0.0147
	5	0.0024	0.0029	0.0017	0.0021	0.0077	0.0112
	6	0.0027	0.003	0.0015	0.0015	0.0024	0.0023
	7	0	0	0	0	0	0
	8	0	0	0	0	0	0
	9	0.0006	0.0008	0.0009	0.0013	0.0031	0.0036
	10	0.0015	0.0018	0.0023	0.0033	0.0058	0.0069
	11	0.0017	0.0021	0.0029	0.0047	0.0066	0.0087
	12	0.0026	0.005	0.0022	0.0041	0.0046	0.0047

TABLE S6

The mean and standard deviation of  $MSE_2$  for GN4, GN8 and GN11 when the true skeleton was used as input. We simulated 25 data sets for each combination of topology,  $N$ , and  $\beta$  and we ran each algorithm once per data set.  $MSE_2$  is calculated only from the true edges.

Method	$N$	$\beta$	$MSE_2$					
			GN4		GN8		GN11	
			mean	sd	mean	sd	mean	sd
baycn	100	0.2	0.2305	0.0351	0.2707	0.0294	0.1743	0.0259
		0.5	0.0987	0.0607	0.0951	0.0401	0.0514	0.0322
		1	0.015	0.0414	0.0286	0.0549	0.0064	0.0047
Gibbs	100	0.2	0.2034	0.0292	0.2483	0.0276	0.1504	0.0215
		0.5	0.1009	0.0286	0.0873	0.0242	0.0439	0.03
		1	0.0221	0.0357	0.0313	0.0518	0.0005	0.0003
MC <sup>3</sup>	100	0.2	0.2039	0.0279	0.2488	0.0283	0.1508	0.0202
		0.5	0.1022	0.0325	0.0888	0.027	0.0438	0.0299
		1	0.1913	0.2189	0.1573	0.124	0.0003	0.0002
order	100	0.2	0.3144	0.0563	0.368	0.0375	0.271	0.0336
		0.5	0.1187	0.0436	0.0997	0.0384	0.0657	0.0374
		1	0.0146	0.0195	0.0309	0.0432	0.0069	0.0023
partition	100	0.2	0.2505	0.0423	0.316	0.025	0.2067	0.0247
		0.5	0.1125	0.0388	0.1202	0.0478	0.0656	0.0329
		1	0.0213	0.023	0.0393	0.05	0.0291	0.0223
baycn	200	0.2	0.1796	0.0484	0.2129	0.0372	0.1308	0.0269
		0.5	0.1132	0.0958	0.1302	0.0792	0.0182	0.0243
		1	0.0069	0.0214	0.0649	0.1041	0.0098	0.0062
Gibbs	200	0.2	0.1716	0.0487	0.2071	0.0345	0.1239	0.0248
		0.5	0.106	0.0683	0.0871	0.031	0.0134	0.0269
		1	0.0015	0.0052	0.0005	0.0018	0.0004	0.0004
MC <sup>3</sup>	200	0.2	0.1725	0.0472	0.2071	0.035	0.1237	0.0252
		0.5	0.1152	0.0966	0.1083	0.0626	0.0133	0.0268
		1	0.2132	0.2264	0.2105	0.1217	0.0003	0.0002
order	200	0.2	0.2743	0.0793	0.2993	0.053	0.2052	0.0459
		0.5	0.1089	0.072	0.0857	0.032	0.0322	0.0327
		1	0.0067	0.0182	0.0051	0.0024	0.0087	0.004
partition	200	0.2	0.2035	0.045	0.2605	0.0325	0.1653	0.0327
		0.5	0.1034	0.0628	0.1136	0.0561	0.0426	0.0259
		1	0.0075	0.0133	0.013	0.0171	0.0327	0.0216
baycn	600	0.2	0.1235	0.0372	0.1721	0.0813	0.0908	0.0288
		0.5	0.0755	0.0903	0.1005	0.0992	0.0071	0.0064
		1	0.0104	0.0273	0.0301	0.0686	0.0068	0.0059
Gibbs	600	0.2	0.125	0.0272	0.1674	0.0724	0.0864	0.0276
		0.5	0.0893	0.0835	0.0651	0.0431	0.0006	0.0012
		1	0	0	0	0	0.0005	0.0004
MC <sup>3</sup>	600	0.2	0.1241	0.0282	0.1683	0.0741	0.0868	0.0274
		0.5	0.229	0.2196	0.1316	0.1398	0.0005	0.0013
		1	0.2311	0.2266	0.2232	0.1151	0.0003	0.0002
order	600	0.2	0.1351	0.0397	0.1648	0.069	0.1055	0.0382
		0.5	0.0891	0.0898	0.0518	0.0433	0.0146	0.0158
		1	0.0018	0.0006	0.0038	0.0005	0.0109	0.0052
partition	600	0.2	0.1257	0.028	0.1665	0.0615	0.1	0.0305
		0.5	0.091	0.0803	0.0736	0.0792	0.0394	0.02
		1	0.001	0.0015	0.0059	0.0146	0.0477	0.0389

Supplementary Tables.

Table S7: The mean and standard deviation of precision, power, and  $MSE_2$  for topology GN4 when a fully connected graph was the input to each algorithm. When calculating precision and power we considered an edge present if the sum of the probability of the two directions was greater than 0.5.

Method	$N$	$\beta$	Precision		Power		$MSE_2$	
			mean	sd	mean	sd	mean	sd
baycn	100	0.2	0.94	0.2077	0.43	0.2654	0.2398	0.0326
		0.5	0.982	0.0627	0.98	0.0692	0.1235	0.0478
		1	0.9707	0.0841	1	0	0.0439	0.0387
Gibbs	100	0.2	0.942	0.206	0.5	0.2602	0.2163	0.0303
		0.5	0.984	0.0554	1	0	0.1212	0.0299
		1	0.9093	0.1184	1	0	0.0938	0.0592
MC <sup>3</sup>	100	0.2	0.942	0.206	0.49	0.265	0.2155	0.0312
		0.5	0.976	0.0663	1	0	0.1215	0.0329
		1	0.9093	0.1184	1	0	0.0945	0.0683
order	100	0.2	0.80	0.4082	0.29	0.2126	0.315	0.0562
		0.5	0.99	0.05	0.96	0.0935	0.1197	0.0502
		1	0.992	0.04	1	0	0.0193	0.0287
partition	100	0.2	0.96	0.2	0.36	0.2051	0.2546	0.04
		0.5	0.982	0.0627	0.98	0.0692	0.1118	0.0357
		1	0.976	0.0663	1	0	0.0287	0.0311
scanBMA	100	0.2	0.88	0.3317	0.35	0.25	-	-
		0.5	0.948	0.0952	0.97	0.0829	-	-
		1	0.7927	0.0281	0.99	0.05	-	-
baycn	200	0.2	0.99	0.05	0.74	0.2222	0.1812	0.0427
		0.5	0.992	0.04	1	0	0.101	0.0769
		1	0.984	0.0554	1	0	0.0307	0.0427
Gibbs	200	0.2	0.98	0.0692	0.77	0.2155	0.1763	0.0383
		0.5	0.992	0.04	1	0	0.1134	0.0555
		1	0.952	0.0872	1	0	0.0521	0.0476
MC <sup>3</sup>	200	0.2	0.98	0.0692	0.77	0.2155	0.1765	0.0376
		0.5	0.992	0.04	1	0	0.1189	0.0619
		1	0.96	0.0816	1	0	0.0525	0.0452
order	200	0.2	0.9067	0.2809	0.48	0.2385	0.2768	0.0782
		0.5	1	0	1	0	0.1072	0.0721
		1	0.992	0.04	1	0	0.011	0.0349
partition	200	0.2	0.9867	0.0667	0.59	0.2026	0.2087	0.0448
		0.5	0.992	0.04	1	0	0.1043	0.0646
		1	0.992	0.04	1	0	0.012	0.0261
scanBMA	200	0.2	0.9787	0.0763	0.67	0.225	-	-
		0.5	0.8747	0.1077	1	0	-	-
		1	0.8	0	1	0	-	-

Method	$N$	$\beta$	Precision		Power		MSE <sub>2</sub>	
			mean	sd	mean	sd	mean	sd
baycn	600	0.2	0.992	0.04	1	0	0.133	0.0358
		0.5	0.992	0.04	1	0	0.0954	0.096
		1	0.992	0.04	1	0	0.0125	0.0102
Gibbs	600	0.2	0.992	0.04	0.99	0.05	0.1274	0.0219
		0.5	0.992	0.04	1	0	0.0982	0.0741
		1	0.992	0.04	1	0	0.0163	0.0156
MC <sup>3</sup>	600	0.2	0.992	0.04	0.99	0.05	0.131	0.0225
		0.5	0.992	0.04	1	0	0.1098	0.093
		1	1	0	1	0	0.0153	0.0124
order	600	0.2	1	0	0.96	0.1181	0.1395	0.0391
		0.5	1	0	1	0	0.0909	0.0903
		1	1	0	1	0	0.002	0.0008
partition	600	0.2	1	0	0.97	0.1099	0.1288	0.0272
		0.5	1	0	1	0	0.0869	0.077
		1	1	0	1	0	0.0016	0.0018
scanBMA	600	0.2	0.976	0.0663	0.99	0.05	-	-
		0.5	0.8	0	1	0	-	-
		1	0.8	0	1	0	-	-



TABLE S8

The posterior probability of the three edge states for baycn and partition MCMC from the first 7 simulated data sets of GN4 with  $N = 100$  and  $\beta = 0.2$ . The edges in red are the false edges, edge numbers with -v are the edges that make a v-structure, and the edge numbers in bold are the edges where baycn inferred a true edge as present but partition MCMC did not.

		Posterior Probability: GN4					
data set	Edge	baycn			partition		
		zero	one	two	zero	one	two
1	1	0.08	0.045	0.875	0.032	0.04	0.928
	2-v	0.12	0.085	0.795	0.045	0.047	0.908
	<b>3</b>	0.025	0.055	0.92	0.03	0.026	0.944
	<b>4</b>	0.08	0.045	0.875	0.044	0.029	0.928
	5	0.265	0.21	0.525	0.173	0.117	0.709
	6-v	0.48	0.515	0.005	0.536	0.463	0.001
2	1	0.435	0.405	0.16	0.405	0.358	0.237
	2-v	0.045	0.075	0.88	0.025	0.027	0.948
	<b>3</b>	0.035	0.1	0.865	0.025	0.04	0.935
	<b>4</b>	0.245	0.32	0.435	0.209	0.289	0.501
	<b>5</b>	0.2	0.36	0.44	0.145	0.244	0.611
	6-v	0.505	0.44	0.055	0.516	0.434	0.05
3	1	0.515	0.385	0.1	0.473	0.349	0.178
	<b>2-v</b>	0.285	0.285	0.43	0.177	0.226	0.597
	<b>3</b>	0.19	0.34	0.47	0.161	0.213	0.626
	<b>4</b>	0.085	0.045	0.87	0.039	0.037	0.924
	5	0.25	0.435	0.315	0.204	0.363	0.433
	6-v	0.15	0.25	0.6	0.126	0.133	0.741
4	1	0.14	0.105	0.755	0.101	0.097	0.802
	2-v	0.185	0.19	0.625	0.126	0.132	0.742
	<b>3</b>	0.055	0.095	0.85	0.051	0.081	0.868
	<b>4</b>	0.085	0.06	0.855	0.056	0.047	0.897
	<b>5</b>	0.455	0.54	0.005	0.511	0.488	0.001
	6-v	0.185	0.18	0.635	0.105	0.121	0.774
5	1	0.16	0.175	0.665	0.142	0.152	0.706
	2-v	0.175	0.115	0.71	0.076	0.06	0.864
	<b>3</b>	0.09	0.09	0.82	0.047	0.031	0.921
	<b>4</b>	0.06	0.095	0.845	0.025	0.026	0.949
	5	0.075	0.06	0.865	0.036	0.052	0.911
	6-v	0.485	0.46	0.055	0.499	0.464	0.037
6	1	0.165	0.25	0.585	0.153	0.132	0.714
	2-v	0.52	0.475	0.005	0.469	0.491	0.04
	<b>3</b>	0.045	0.08	0.875	0.032	0.04	0.928
	<b>4</b>	0.03	0.025	0.945	0.03	0.029	0.941
	5	0.1	0.125	0.775	0.066	0.057	0.877
	6-v	0.06	0.035	0.905	0.036	0.022	0.941
7	1	0.48	0.43	0.09	0.416	0.383	0.201
	2-v	0.065	0.085	0.85	0.05	0.045	0.905
	<b>3</b>	0.05	0.05	0.9	0.039	0.06	0.901
	<b>4</b>	0.11	0.04	0.85	0.059	0.024	0.918
	5	0.145	0.18	0.675	0.097	0.117	0.786
	6-v	0.16	0.2	0.64	0.13	0.116	0.754

TABLE S9

The posterior probability of the three edge states for baycn and partition MCMC from the first 7 simulated data sets of GN4 with  $N = 200$  and  $\beta = 0.2$ . The edges in red are the false edges, edge numbers with -v are the edges that make a v-structure, and the edge numbers in bold are the edges where baycn inferred a true edge as present but partition MCMC did not.

		Posterior Probability: GN4					
data set	Edge	baycn			partition		
		zero	one	two	zero	one	two
1	1	0.415	0.38	0.205	0.389	0.257	0.354
	2-v	0.425	0.515	0.06	0.419	0.459	0.122
	<b>3</b>	0.095	0.045	0.86	0.037	0.032	0.93
	<b>4</b>	0.075	0.09	0.835	0.037	0.054	0.909
	5	0.14	0.115	0.745	0.056	0.091	0.853
	6-v	0.605	0.395	0	0.599	0.392	0.01
2	1	0.33	0.67	0	0.272	0.728	0
	2-v	0.335	0.645	0.02	0.231	0.692	0.077
	<b>3</b>	0.03	0.075	0.895	0.015	0.031	0.954
	<b>4</b>	0.23	0.16	0.61	0.121	0.079	0.8
	<b>5</b>	0.37	0.34	0.29	0.204	0.172	0.623
	6-v	0.525	0.475	0	0.475	0.509	0.016
3	1	0.37	0.385	0.245	0.298	0.294	0.408
	<b>2-v</b>	0.32	0.285	0.395	0.218	0.19	0.592
	<b>3</b>	0.025	0.07	0.905	0.02	0.016	0.964
	<b>4</b>	0.13	0.085	0.785	0.072	0.065	0.863
	5	0.335	0.535	0.13	0.349	0.43	0.221
	6-v	0.32	0.44	0.24	0.253	0.286	0.461
4	1	0.11	0.13	0.76	0.07	0.051	0.879
	<b>2-v</b>	0.415	0.29	0.295	0.3	0.181	0.519
	<b>3</b>	0.135	0.07	0.795	0.052	0.046	0.901
	<b>4</b>	0.115	0.19	0.695	0.076	0.125	0.799
	5	0.235	0.25	0.515	0.141	0.188	0.671
	6-v	0.385	0.525	0.09	0.378	0.461	0.161
5	1	0.51	0.48	0.01	0.498	0.47	0.032
	2-v	0.41	0.4	0.19	0.383	0.312	0.305
	<b>3</b>	0.035	0.045	0.92	0.019	0.021	0.96
	<b>4</b>	0.045	0.035	0.92	0.016	0.021	0.963
	5	0.505	0.485	0.01	0.484	0.494	0.022
	6-v	0.335	0.385	0.28	0.231	0.304	0.465
6	1	0.225	0.17	0.605	0.146	0.103	0.751
	2-v	0.56	0.44	0	0.591	0.403	0.006
	<b>3</b>	0.4	0.48	0.12	0.47	0.367	0.163
	<b>4</b>	0.03	0.05	0.92	0.021	0.02	0.959
	5	0.34	0.605	0.055	0.31	0.562	0.127
	<b>6-v</b>	0.285	0.295	0.42	0.17	0.19	0.641
7	<b>1</b>	0.335	0.36	0.305	0.248	0.233	0.519
	<b>2-v</b>	0.27	0.235	0.495	0.166	0.157	0.677
	<b>3</b>	0.075	0.035	0.89	0.02	0.019	0.961
	<b>4</b>	0.105	0.12	0.775	0.059	0.082	0.859
	5	0.325	0.46	0.215	0.234	0.406	0.359
	6-v	0.425	0.575	0	0.439	0.546	0.015

TABLE S10

The posterior probability of the three edge states for baycn and partition MCMC from the first 7 simulated data sets of GN4 with  $N = 600$  and  $\beta = 0.2$ . The edges in red are the false edges, edge numbers with -v are the edges that make a v-structure, and the edge numbers in bold are the edges where baycn inferred a true edge as present but partition MCMC did not.

		Posterior Probability: GN4					
data set	Edge	baycn			partition		
		zero	one	two	zero	one	two
1	1	0.61	0.39	0	0.511	0.489	0
	<b>2-v</b>	0.345	0.325	0.33	0.224	0.148	0.627
	3	0.065	0.03	0.905	0.02	0.012	0.968
	4	0.065	0.045	0.89	0.016	0.016	0.968
	5	0.405	0.595	0	0.491	0.509	0
	<b>6-v</b>	0.29	0.26	0.45	0.091	0.142	0.767
2	1	0.61	0.39	0	0.632	0.368	0
	2-v	0.585	0.415	0	0.641	0.359	0
	3	0.025	0.055	0.92	0.009	0.014	0.978
	4	0.05	0.05	0.9	0.017	0.014	0.969
	5	0.36	0.64	0	0.424	0.576	0
	6-v	0.445	0.555	0	0.401	0.589	0.01
3	1	0.63	0.37	0	0.615	0.385	0
	2-v	0.465	0.465	0.07	0.379	0.384	0.237
	3	0.13	0.095	0.775	0.037	0.034	0.929
	4	0.095	0.15	0.755	0.019	0.03	0.951
	5	0.44	0.56	0	0.426	0.574	0
	6-v	0.645	0.355	0	0.54	0.46	0
4	1	0.57	0.43	0	0.469	0.53	0.001
	2-v	0.555	0.39	0.055	0.368	0.431	0.201
	3	0.065	0.065	0.87	0.007	0.01	0.983
	4	0.085	0.055	0.86	0.007	0.01	0.983
	5	0.63	0.37	0	0.505	0.495	0
	6-v	0.45	0.55	0	0.495	0.505	0
5	1	0.545	0.455	0	0.586	0.414	0
	2-v	0.515	0.485	0	0.602	0.392	0.006
	3	0.025	0.045	0.93	0.007	0.006	0.986
	4	0.065	0.04	0.895	0.012	0.01	0.978
	5	0.525	0.475	0	0.439	0.559	0.002
	6-v	0.355	0.645	0	0.425	0.575	0
6	1	0.765	0.23	0.005	0.758	0.233	0.009
	2-v	0.645	0.355	0	0.682	0.314	0.004
	3	0.15	0.07	0.78	0.02	0.015	0.965
	4	0.06	0.05	0.89	0.007	0.006	0.986
	5	0.33	0.67	0	0.232	0.768	0
	6-v	0.375	0.625	0	0.283	0.711	0.006
7	1	0.425	0.575	0	0.46	0.54	0
	2-v	0.4	0.6	0	0.5	0.5	0
	3	0.055	0.06	0.885	0.006	0.012	0.981
	4	0.06	0.06	0.88	0.012	0.017	0.97
	5	0.5	0.5	0	0.569	0.431	0
	6-v	0.45	0.55	0	0.534	0.46	0.006

TABLE S11

Posterior probabilities from baycn on the GEUVADIS eQTL-gene set Q8 with five associated PCs included in the network as confounding variables. A fully connected graph (excluding the edges between PC nodes) was used as the input to baycn. The rows highlighted in yellow indicate the edges between the nodes of interest.

edge	zero	one	two
rs11305802-TMEM55B	0.170	0.000	0.830
rs11305802-RP11-203M5.8	0.805	0.000	0.195
rs11305802-PNP	1.000	0.000	0.000
rs11305802-PC1	0.240	0.000	0.760
rs11305802-PC2	0.195	0.000	0.805
rs11305802-PC6	0.255	0.000	0.745
rs11305802-PC7	0.125	0.000	0.875
rs11305802-PC9	0.370	0.000	0.630
TMEM55B-RP11-203M5.8	0.150	0.820	0.030
TMEM55B-PNP	0.330	0.670	0.000
TMEM55B-PC1	0.385	0.615	0.000
TMEM55B-PC2	0.085	0.550	0.365
TMEM55B-PC6	0.015	0.055	0.930
TMEM55B-PC7	0.050	0.030	0.920
TMEM55B-PC9	0.260	0.730	0.010
RP11-203M5.8-PNP	0.760	0.240	0.000
RP11-203M5.8-PC1	0.075	0.145	0.780
RP11-203M5.8-PC2	0.085	0.240	0.675
RP11-203M5.8-PC6	0.315	0.685	0.000
RP11-203M5.8-PC7	0.175	0.115	0.710
RP11-203M5.8-PC9	0.035	0.060	0.905
PNP-PC1	0.190	0.715	0.095
PNP-PC2	0.135	0.845	0.020
PNP-PC6	0.040	0.065	0.895
PNP-PC7	0.565	0.180	0.255
PNP-PC9	0.165	0.695	0.140

TABLE S12

Posterior probabilities from order MCMC on the GEUVADIS eQTL-gene set Q8 with associated PCs. A fully connected graph (excluding the edges between PC nodes) was used as the input.

edge	zero	one	two
rs11305802-TMEM55B	0.00	0.00	1.00
rs11305802-RP11-203M5.8	0.25	0.00	0.75
rs11305802-PNP	1.00	0.00	0.00
rs11305802-PC1	0.00	0.00	1.00
rs11305802-PC2	0.00	0.00	1.00
rs11305802-PC6	0.00	0.00	1.00
rs11305802-PC7	0.00	0.00	1.00
rs11305802-PC9	0.00	0.00	1.00
TMEM55B-RP11-203M5.8	0.37	0.63	-0.00
TMEM55B-PNP	0.08	0.92	0.00
TMEM55B-PC1	0.00	0.00	1.00
TMEM55B-PC2	0.00	0.00	1.00
TMEM55B-PC6	0.00	0.00	1.00
TMEM55B-PC7	0.00	0.00	1.00
TMEM55B-PC9	0.00	0.00	1.00
RP11-203M5.8-PNP	0.25	0.75	0.00
RP11-203M5.8-PC1	0.00	0.00	1.00
RP11-203M5.8-PC2	0.00	0.00	1.00
RP11-203M5.8-PC6	0.00	0.22	0.78
RP11-203M5.8-PC7	0.00	0.00	1.00
RP11-203M5.8-PC9	0.00	0.00	1.00
PNP-PC1	0.00	0.00	1.00
PNP-PC2	0.00	0.00	1.00
PNP-PC6	0.00	0.00	1.00
PNP-PC7	0.00	0.00	1.00
PNP-PC9	0.00	0.00	1.00

TABLE S13

Posterior probabilities from partition MCMC on the GEUVADIS eQTL-gene set Q8 with associated PCs. A fully connected graph (excluding the edges between PC nodes) was used as the input.

edge	zero	one	two
rs11305802-TMEM55B	0.02	0.00	0.98
rs11305802-RP11-203M5.8	0.32	0.00	0.68
rs11305802-PNP	1.00	0.00	0.00
rs11305802-PC1	0.00	0.00	1.00
rs11305802-PC2	0.00	0.00	1.00
rs11305802-PC6	0.00	0.00	1.00
rs11305802-PC7	0.00	0.00	1.00
rs11305802-PC9	0.00	0.00	1.00
TMEM55B-RP11-203M5.8	0.34	0.51	0.16
TMEM55B-PNP	0.06	0.94	0.00
TMEM55B-PC1	0.15	0.00	0.85
TMEM55B-PC2	0.00	0.00	1.00
TMEM55B-PC6	0.00	0.00	1.00
TMEM55B-PC7	0.00	0.00	1.00
TMEM55B-PC9	0.00	0.04	0.96
RP11-203M5.8-PNP	0.22	0.78	0.00
RP11-203M5.8-PC1	0.00	0.00	1.00
RP11-203M5.8-PC2	0.00	0.00	1.00
RP11-203M5.8-PC6	0.34	0.26	0.40
RP11-203M5.8-PC7	0.00	0.00	1.00
RP11-203M5.8-PC9	0.00	0.00	1.00
PNP-PC1	0.00	0.01	0.99
PNP-PC2	0.00	0.00	1.00
PNP-PC6	0.00	0.00	1.00
PNP-PC7	0.00	0.00	1.00
PNP-PC9	0.00	0.00	1.00

TABLE S14

Posterior probabilities from scanBMA on the GEUVADIS eQTL-gene set Q8 with associated PCs. A fully connected graph (excluding the edges between PC nodes) was used as the input.

edge	zero	one	two
rs11305802-TMEM55B	0.00	0.00	NA
rs11305802-RP11-203M5.8	0.07	0.00	NA
rs11305802-PNP	1.00	0.00	NA
rs11305802-PC1	0.07	0.00	NA
rs11305802-PC2	0.00	0.00	NA
rs11305802-PC6	0.20	0.00	NA
rs11305802-PC7	0.00	0.00	NA
rs11305802-PC9	0.27	0.00	NA
TMEM55B-RP11-203M5.8	0.84	0.80	NA
TMEM55B-PNP	1.00	1.00	NA
TMEM55B-PC1	1.00	1.00	NA
TMEM55B-PC2	0.28	0.23	NA
TMEM55B-PC6	0.00	0.00	NA
TMEM55B-PC7	0.00	0.00	NA
TMEM55B-PC9	0.94	1.00	NA
RP11-203M5.8-PNP	1.00	1.00	NA
RP11-203M5.8-PC1	0.00	0.00	NA
RP11-203M5.8-PC2	0.50	0.77	NA
RP11-203M5.8-PC6	1.00	1.00	NA
RP11-203M5.8-PC7	0.12	0.00	NA
RP11-203M5.8-PC9	0.02	0.03	NA
PNP-PC1	0.19	0.68	NA
PNP-PC2	0.76	0.93	NA
PNP-PC6	0.04	0.00	NA
PNP-PC7	0.57	0.17	NA
PNP-PC9	0.61	0.96	NA

TABLE S15

Posterior probabilities from baycn on the GEUVADIS eQTL-gene set Q8 without the associated PCs. A fully connected graph was used as the input.

edge	zero	one	two
rs11305802-TMEM55B	0.210	0.000	0.79
rs11305802-RP11-203M5.8	0.410	0.000	0.59
rs11305802-PNP	1.000	0.000	0.00
TMEM55B-RP11-203M5.8	0.525	0.465	0.01
TMEM55B-PNP	0.155	0.845	0.00
RP11-203M5.8-PNP	0.185	0.815	0.00

TABLE S16

Posterior probabilities from baycn on the GEUVADIS eQTL-gene set Q20. A fully connected graph was used as the input.

edge	zero	one	two
rs142060986-RP11292F9.1	0	0	1
rs142060986-FAM27E1	1	0	0
RP11292F9.1-FAM27E1	0	1	0



TABLE S17

Posterior probabilities from baycn for the GEUVADIS eQTL-gene set Q21 with two PCs are included in the network as confounding variables. A fully connected graph was used as the input. The rows highlighted in yellow indicate the edges between the nodes of interest.

edge	zero	one	two
rs147156488-FAM27C	0.000	0.000	1.000
rs147156488-FAM27A	0.000	0.000	1.000
rs147156488-FAM27D1	1.000	0.000	0.000
rs147156488-PC1	1.000	0.000	0.000
rs147156488-PC3	1.000	0.000	0.000
FAM27C-FAM27A	0.510	0.030	0.460
FAM27C-FAM27D1	0.000	1.000	0.000
FAM27C-PC1	0.250	0.030	0.720
FAM27C-PC3	0.180	0.140	0.680
FAM27A-FAM27D1	0.000	0.510	0.490
FAM27A-PC1	0.145	0.050	0.805
FAM27A-PC3	0.555	0.115	0.330
FAM27D1-PC1	0.245	0.220	0.535
FAM27D1-PC3	0.160	0.125	0.715

TABLE S18

Posterior probabilities from baycn on the GEUVADIS eQTL-gene set Q23 with two PCs included in the network as confounding variables. A fully connected graph was used as input. The rows highlighted in yellow indicate the edges between the nodes of interest.

edge	zero	one	two
rs150605045-AGAP9	1.000	0.000	0.000
rs150605045-AGAP10	1.000	0.000	0.000
rs150605045-PC1	1.000	0.000	0.000
rs150605045-PC8	1.000	0.000	0.000
AGAP9-AGAP10	0.720	0.280	0.000
AGAP9-PC1	0.595	0.385	0.020
AGAP9-PC8	0.495	0.455	0.050
AGAP10-PC1	0.065	0.065	0.870
AGAP10-PC8	0.035	0.080	0.885

TABLE S19

Posterior probabilities from baycn on the GEUVADIS eQTL-gene set Q37 with one PC included in the network as a confounding variable. A fully connected graph was used as input. The rows highlighted in yellow indicate the edges between the nodes of interest.

edge	zero	one	two
rs3858954-GOLGA6L19	0.660	0.000	0.340
rs3858954-GOLGA6L9	0.335	0.000	0.665
rs3858954-GOLGA6L20	0.965	0.000	0.035
rs3858954-PC1	0.100	0.000	0.900
GOLGA6L19-GOLGA6L9	0.035	0.055	0.910
GOLGA6L19-GOLGA6L20	0.335	0.665	0.000
GOLGA6L19-PC1	0.665	0.210	0.125
GOLGA6L9-GOLGA6L20	0.175	0.825	0.000
GOLGA6L9-PC1	0.110	0.030	0.860
GOLGA6L20-PC1	0.135	0.050	0.815

TABLE S20

Posterior probabilities from baycn on the GEUVADIS eQTL-gene set Q50 with two PCs included in the network as confounding variables. A fully connected graph was used as input. The rows highlighted in yellow indicate the edges between the nodes of interest.

edge	zero	one	two
rs7124238-SBF2-AS1	0.195	0.000	0.805
rs7124238-SWAP70	1.000	0.000	0.000
rs7124238-PC1	0.135	0.000	0.865
rs7124238-PC5	0.465	0.000	0.535
SBF2-AS1-SWAP70	0.035	0.965	0.000
SBF2-AS1-PC1	0.035	0.020	0.945
SBF2-AS1-PC5	0.015	0.040	0.945
SWAP70-PC1	0.550	0.415	0.035
SWAP70-PC5	0.280	0.720	0.000

TABLE S21

Posterior probabilities from baycn on the GEUVADIS eQTL-gene set Q62. A fully connected graph was used as input.

edge	zero	one	two
rs9426902-S100A6	0.845	0.00	0.155
rs9426902-S100A4	0.420	0.00	0.580
S100A6-S100A4	0.720	0.28	0.000

Table S22: Posterior probability for each edge state for baycn, order MCMC, partition MCMC, and scanBMA on the *Drosophila* data.

edge	baycn			order MCMC			partition MCMC			scanBMA		
	zero	one	two	zero	one	two	zero	one	two	zero	one	two
Meso-Twi_2_4h	0.282	0.644	0.074	0.026	0.747	0.227	0.084	0.385	0.531	0.248	0.800	NA
VM-Bin_6_8h	0.126	0.462	0.412	0.006	0.161	0.833	0.004	0.388	0.608	0.032	0.208	NA
VM-Bin_8_10h	0.172	0.474	0.354	0.087	0.677	0.236	0.012	0.387	0.601	0.392	0.913	NA
VM-Bin_10_12h	0.076	0.054	0.870	0.000	0.000	1.000	0.000	0.030	0.970	0.000	0.000	NA
SM-Mef2_10_12h	0.440	0.208	0.352	0.000	0.000	1.000	0.046	0.062	0.892	0.321	0.235	NA
CM-Bin_10_12h	0.420	0.196	0.384	0.000	0.000	1.000	0.075	0.081	0.844	0.767	0.327	NA
Meso_SM-Tin_2_4h	0.102	0.534	0.364	0.212	0.163	0.625	0.027	0.395	0.577	0.296	0.757	NA
Meso_SM-Tin_4_6h	0.024	0.164	0.812	0.004	0.027	0.969	0.011	0.087	0.901	0.000	0.000	NA
Meso_SM-Tin_6_8h	0.180	0.040	0.780	0.000	0.000	1.000	0.005	0.004	0.991	0.000	0.000	NA
Meso_SM-Mef2_2_4h	0.226	0.556	0.218	0.002	0.389	0.608	0.059	0.337	0.605	1.000	1.000	NA
Meso_SM-Mef2_4_6h	0.174	0.282	0.544	0.004	0.392	0.605	0.016	0.313	0.671	0.094	0.062	NA
Meso_SM-Mef2_6_8h	0.024	0.050	0.926	0.000	0.000	1.000	0.001	0.000	0.999	0.000	0.000	NA
Meso_SM-Mef2_8_10h	0.052	0.056	0.892	0.000	0.000	1.000	0.002	0.007	0.990	0.000	0.000	NA
Meso_SM-Mef2_10_12h	0.036	0.048	0.916	0.000	0.000	1.000	0.007	0.010	0.983	0.000	0.000	NA
VM_SM-Bin_10_12h	0.504	0.282	0.214	0.000	0.000	1.000	0.000	0.000	1.000	0.640	0.787	NA
VM_SM-Twi_2_4h	0.378	0.622	0.000	0.180	0.820	0.000	0.707	0.288	0.005	0.734	0.526	NA
VM_SM-Mef2_10_12h	0.738	0.262	0.000	0.712	0.288	0.000	0.414	0.579	0.007	1.000	1.000	NA
Tin_2_4h-Tin_4_6h	0.332	0.668	0.000	0.461	0.539	0.000	0.943	0.057	0.000	1.000	1.000	NA
Tin_2_4h-Twi_4_6h	0.526	0.464	0.010	0.197	0.349	0.454	0.001	0.945	0.054	0.970	1.000	NA
Tin_4_6h-Twi_4_6h	0.548	0.382	0.070	0.362	0.094	0.545	0.001	0.055	0.944	0.219	0.342	NA
Tin_4_6h-Twi_6_8h	0.522	0.476	0.002	0.445	0.448	0.107	0.000	0.944	0.056	1.000	1.000	NA
Tin_4_6h-Mef2_2_4h	0.932	0.066	0.002	0.939	0.016	0.045	0.796	0.000	0.204	0.780	0.167	NA
Tin_4_6h-Mef2_4_6h	0.972	0.028	0.000	0.675	0.090	0.236	0.002	0.057	0.940	1.000	0.952	NA
Tin_6_8h-Bin_6_8h	0.300	0.576	0.124	0.559	0.056	0.385	0.247	0.000	0.753	0.921	0.682	NA
Tin_6_8h-Bap_6_8h	0.494	0.506	0.000	0.894	0.106	0.000	0.980	0.020	0.000	1.000	1.000	NA
Bin_6_8h-Bin_8_10h	0.604	0.396	0.000	0.546	0.454	0.000	0.961	0.039	0.000	1.000	1.000	NA
Bin_6_8h-Bin_10_12h	0.494	0.408	0.098	0.000	0.000	1.000	0.001	0.000	0.999	0.973	1.000	NA
Bin_6_8h-Bap_6_8h	0.746	0.216	0.038	0.030	0.355	0.615	0.009	0.761	0.231	0.974	0.571	NA
Bin_8_10h-Bin_10_12h	0.500	0.500	0.000	0.894	0.106	0.000	1.000	0.000	0.000	1.000	1.000	NA
Twi_2_4h-Twi_4_6h	0.224	0.776	0.000	0.319	0.680	0.001	0.556	0.443	0.001	1.000	1.000	NA
Twi_4_6h-Twi_6_8h	0.400	0.596	0.004	0.509	0.145	0.347	0.678	0.318	0.004	1.000	1.000	NA
Twi_4_6h-Mef2_4_6h	0.992	0.008	0.000	0.640	0.360	0.000	0.772	0.228	0.000	1.000	1.000	NA
Twi_6_8h-Mef2_6_8h	0.890	0.110	0.000	0.824	0.176	0.000	0.642	0.358	0.000	1.000	1.000	NA
Mef2_2_4h-Mef2_6_8h	0.604	0.284	0.112	0.002	0.005	0.993	0.015	0.126	0.859	0.170	0.686	NA
Mef2_2_4h-Mef2_10_12h	0.310	0.610	0.080	0.175	0.782	0.044	0.041	0.607	0.352	0.705	0.891	NA
Mef2_4_6h-Mef2_6_8h	0.008	0.992	0.000	0.107	0.125	0.768	0.054	0.946	0.000	1.000	1.000	NA
Mef2_6_8h-Mef2_8_10h	0.624	0.376	0.000	0.138	0.862	0.000	0.264	0.736	0.000	1.000	1.000	NA
Mef2_8_10h-Mef2_10_12h	0.172	0.828	0.000	0.137	0.863	0.000	0.455	0.545	0.000	1.000	1.000	NA

TABLE S24

Posterior probabilities inferred by baycn for the *Drosophila* data set. The graph output from MRPC was used as the input to baycn with the addition of the edges: VM-bin\_6.8, VM-bin\_10.12, Meso\_SM-tin\_4.6, Meso\_SM-tin\_6.8, Meso\_SM-mef2\_4.6, Meso\_SM-mef2\_6.8, Meso\_SM-mef2\_8.10, and Meso\_SM-mef2\_10.12.

edge	Posterior Probability		
	zero	one	two
Meso-twi_2.4	0.282	0.644	0.074
VM-bin_6.8	0.126	0.462	0.412
VM-bin_8.10	0.172	0.474	0.354
VM-bin_10.12	0.076	0.054	0.870
SM-mef2_10.12	0.440	0.208	0.352
CM-bin_10.12	0.420	0.196	0.384
Meso_SM-tin_2.4	0.102	0.534	0.364
Meso_SM-tin_4.6	0.024	0.164	0.812
Meso_SM-tin_6.8	0.180	0.040	0.780
Meso_SM-mef2_2.4	0.226	0.556	0.218
Meso_SM-mef2_4.6	0.174	0.282	0.544
Meso_SM-mef2_6.8	0.024	0.050	0.926
Meso_SM-mef2_8.10	0.052	0.056	0.892
Meso_SM-mef2_10.12	0.036	0.048	0.916
VM_SM-bin_10.12	0.504	0.282	0.214
VM_SM-twi_2.4	0.378	0.622	0.000
VM_SM-mef2_10.12	0.738	0.262	0.000
tin_2.4-tin_4.6	0.332	0.668	0.000
tin_2.4-twi_4.6	0.526	0.464	0.010
tin_4.6-twi_4.6	0.548	0.382	0.070
tin_4.6-twi_6.8	0.522	0.476	0.002
tin_4.6-mef2_2.4	0.932	0.066	0.002
tin_4.6-mef2_4.6	0.972	0.028	0.000
tin_6.8-bin_6.8	0.300	0.576	0.124
tin_6.8-bap_6.8	0.494	0.506	0.000
bin_6.8-bin_8.10	0.604	0.396	0.000
bin_6.8-bin_10.12	0.494	0.408	0.098
bin_6.8-bap_6.8	0.746	0.216	0.038
bin_8.10-bin_10.12	0.500	0.500	0.000
twi_2.4-twi_4.6	0.224	0.776	0.000
twi_4.6-twi_6.8	0.400	0.596	0.004
twi_4.6-mef2_4.6	0.992	0.008	0.000
twi_6.8-mef2_6.8	0.890	0.110	0.000
mef2_2.4-mef2_6.8	0.604	0.284	0.112
mef2_2.4-mef2_10.12	0.310	0.610	0.080
mef2_4.6-mef2_6.8	0.008	0.992	0.000
mef2_6.8-mef2_8.10	0.624	0.376	0.000
mef2_8.10-mef2_10.12	0.172	0.828	0.000

## REFERENCES

- BADSHA, M. B. and FU, A. Q. (2019). Learning causal biological networks with the principle of Mendelian randomization. *Frontiers in Genetics* **10** 460.
- BADSHA, M. B., MARTIN, E. A. and FU, A. Q. (2021). MRPC: An R package for inference of causal graphs. *Frontiers in Genetics* **12** 632.
- CASTELLETTI, F. and CONSONNI, G. (2019). Objective Bayes model selection of Gaussian interventional essential graphs for the identification of signaling pathways. *The Annals of Applied Statistics* **13** 2289–2311.

Table S23: Posterior probability for each edge state for baycn, order MCMC, partition MCMC, and scanBMA on the Q8 network from GEUVADIS. All possible edges were input to each method.

edges	baycn			order MCMC			partition MCMC			scanBMA		
	zero	one	two	zero	one	two	zero	one	two	zero	one	two
rs11305802-TMEM55B	0.210	0.00	0.79	0.002	0.000	0.998	0.027	0.000	0.973	0.000	0.000	NA
rs11305802-RP11-203M5.8	0.410	0.00	0.59	0.089	0.000	0.911	0.177	0.000	0.823	0.063	0.072	NA
rs11305802-PNP	1.000	0.00	0.000	1.000	0.000	0.000	1.000	0.000	0.000	1.000	1.000	NA
TMEM55B-RP11-203M5.8	0.525	0.465	0.01	0.445	0.555	0.000	0.423	0.424	0.153	0.844	0.850	NA
TMEM55B-PNP	0.155	0.845	0.000	0.040	0.960	0.000	0.025	0.975	0.000	1.000	1.000	NA
RP11-203M5.8-PNP	0.185	0.815	0.000	0.089	0.911	0.000	0.064	0.936	0.000	1.000	1.000	NA

- CASTELLETTI, F. and CONSONNI, G. (2020). Discovering causal structures in Bayesian Gaussian directed acyclic graph models. *Journal of the Royal Statistical Society: Series A (Statistics in Society)* **183** 1727–1745.
- CASTELLETTI, F. and MASCARO, A. (2022). BCDAG: An R package for Bayesian structure and Causal learning of Gaussian DAGs. *arXiv*. arXiv:2201.12003.
- CASTELLETTI, F. and PELUSO, S. (2022). Network structure learning under uncertain interventions. *Journal of the American Statistical Association* 1–12.
- CHEUNG, V. G. and SPIELMAN, R. S. (2009). Genetics of human gene expression: mapping DNA variants that influence gene expression. *Nature Reviews Genetics* **10** 595–604.
- DAVEY SMITH, G. and HEMANI, G. (2014). Mendelian randomization: genetic anchors for causal inference in epidemiological studies. *Human Molecular Genetics* **23** R89–R98.
- DAVIDSON, E. H. (2010). Emerging properties of animal gene regulatory networks. *Nature* **468** 911–920.
- DAWID, A. P. (2010). Beware of the DAG! In *JMLR Workshop and Conference Proceedings* 59–86.
- EMDIN, C. A., KHERA, A. V. and KATHIRESAN, S. (2017). Mendelian randomization. *Journal of American Medical Association* **318** 1925–1926.
- FRIEDMAN, N. (2004). Inferring cellular networks using probabilistic graphical models. *Science* **303** 799–805.
- FRIEDMAN, N. and KOLLER, D. (2003). Being Bayesian about network structure. A Bayesian approach to structure discovery in Bayesian networks. *Machine Learning* **50** 95–125.
- FRONCZUK, M., RAFTERY, A. E. and YEUNG, K. Y. (2015). CyNetworkBMA: a Cytoscape app for inferring gene regulatory networks. *Source Code for Biology and Medicine* **10** 1–7.
- GIUDICI, P. and CASTELO, R. (2003). Improving Markov chain Monte Carlo model search for data mining. *Machine Learning* **50** 127–158.
- GOMEZ, S. M., NOBLE, W. S. and RZHETSKY, A. (2003). Learning to predict protein–protein interactions from protein sequences. *Bioinformatics* **19** 1875–1881.
- GOUDIE, R. J. and MUKHERJEE, S. (2016). A Gibbs sampler for learning DAGs. *The Journal of Machine Learning Research* **17** 1032–1070.
- GRZEGORCZYK, M. and HUSMEIER, D. (2008). Improving the structure MCMC sampler for Bayesian networks by introducing a new edge reversal move. *Machine Learning* **71** 265.
- GUELZIM, N., BOTTANI, S., BOURGINE, P. and KÉPÈS, F. (2002). Topological and causal structure of the yeast transcriptional regulatory network. *Nature Genetics* **31** 60–63.
- GUYON, I., JANZING, D. and SCHÖLKOPF, B. (2010). Causality: Objectives and Assessment. In *JMLR Workshop and Conference Proceedings* 1–38.
- HE, Y., JIA, J., YU, B. et al. (2013). Reversible MCMC on Markov equivalence classes of sparse directed acyclic graphs. *The Annals of Statistics* **41** 1742–1779.
- HOLM, S. (1979). A simple sequentially rejective multiple test procedure. *Scandinavian Journal of Statistics* 65–70.
- HUNG, L.-H., SHI, K., WU, M. et al. (2017). fastBMA: scalable network inference and transitive reduction. *Giga-Science* **6** gix078.
- KALISCH, M., MÄCHLER, M., COLOMBO, D. et al. (2012). Causal inference using graphical models with the R package pcalg. *Journal of Statistical Software* **47** 1–26.
- KUIPERS, J. and MOFFA, G. (2017). Partition MCMC for inference on acyclic digraphs. *Journal of the American Statistical Association* **112** 282–299.
- KUIPERS, J., SUTER, P. and MOFFA, G. (2022). Efficient sampling and structure learning of Bayesian networks. *Journal of Computational and Graphical Statistics* 1–12.
- LAPPALAINEN, T., SAMMETH, M., FRIEDLÄNDER, M. R. et al. (2013). Transcriptome and genome sequencing uncovers functional variation in humans. *Nature* **501** 506–511.
- LEDAY, G. G. and RICHARDSON, S. (2019). Fast Bayesian inference in large Gaussian graphical models. *Biometrics* **75** 1288–1298.
- LO, K., RAFTERY, A. E., DOMBEK, K. M. et al. (2012). Integrating external biological knowledge in the construction of regulatory networks from time-series expression data. *BMC Systems Biology* **6** 101.
- MADIGAN, D., YORK, J. and ALLARD, D. (1995). Bayesian graphical models for discrete data. *International Statistical Review/Revue Internationale de Statistique* **63** 215–232.
- MCGUIRE, A. L., GABRIEL, S., TISHKOFF, S. A. et al. (2020). The road ahead in genetics and genomics. *Nature Reviews Genetics* **21** 581–596.
- MOHAMMADI, A., WIT, E. C. et al. (2015). Bayesian structure learning in sparse Gaussian graphical models. *Bayesian Analysis* **10** 109–138.
- RAU, A., JAFFRÉZIC, F., FOULLEY, J.-L. and DOERGE, R. W. (2012). Reverse engineering gene regulatory networks using approximate Bayesian computation. *Statistics and Computing* **22** 1257–1271.
- REZAEI TABAR, V., ZAREIFARD, H., SALIMI, S. and PLEWCZYNSKI, D. (2019). An empirical Bayes approach for learning directed acyclic graph using MCMC algorithm. *Statistical Analysis and Data Mining: The ASA Data Science Journal* **12** 394–403.

- SANDERSON, E., GLYMOUR, M. M., HOLMES, M. V. et al. (2022). Mendelian randomization. *Nature Reviews Methods Primers* **2** 6.
- SCHWALLER, L., ROBIN, S. and STUMPF, M. (2019). Closed-form Bayesian inference of graphical model structures by averaging over trees. *Journal de la Société Française de Statistique* **160** 1–23.
- SCUTARI, M. (2010). Learning Bayesian Networks with the bnlearn R Package. *Journal of Statistical Software* **35**. doi:10.18637/jss.v035.i03.
- SEVERINI, T. A. (2000). *Likelihood methods in statistics*. Oxford University Press Ch 9.
- SPIRITES, P., GLYMOUR, C. N. and SCHEINES, R. (2000). *Causation, Prediction, and Search*. MIT Press.
- STEGLE, O., PARTS, L., PIPARI, M. et al. (2012). Using probabilistic estimation of expression residuals (PEER) to obtain increased power and interpretability of gene expression analyses. *Nature Protocols* **7** 500–507.
- STOJNIC, R., FU, A. Q. and ADRYAN, B. (2012). A graphical modelling approach to the dissection of highly correlated transcription factor binding site profiles. *PLoS Computational Biology* **8**.
- SU, C. and BORSUK, M. E. (2016). Improving structure MCMC for Bayesian networks through Markov blanket resampling. *The Journal of Machine Learning Research* **17** 4042–4061.
- VENTURA, L. and RACUGNO, W. (2016). Pseudo-likelihoods for Bayesian inference. In *Topics on Methodological and Applied Statistical Inference* 205–220. Springer.
- VERMA, T. and PEARL, J. (1990). Equivalence and synthesis of causal models. In *Proceedings of the Sixth Annual Conference on Uncertainty in Artificial Intelligence* 255–270. Elsevier Science Inc.
- VIINIKKA, J. and KOIVISTO, M. (2020). Layering-MCMC for Structure Learning in Bayesian Networks. In *Conference on Uncertainty in Artificial Intelligence* 839–848. PMLR.
- VILLAR, D., FLICEK, P. and ODOM, D. T. (2014). Evolution of transcription factor binding in metazoans—mechanisms and functional implications. *Nature Reviews Genetics* **15** 221–233.
- YEUNG, K. Y., DOMBEK, K. M., LO, K. et al. (2011). Construction of regulatory networks using expression time-series data of a genotyped population. *Proceedings of the National Academy of Sciences* **108** 19436–19441.
- YOUNG, W. C., RAFTERY, A. E. and YEUNG, K. Y. (2014). Fast Bayesian inference for gene regulatory networks using ScanBMA. *BMC Systems Biology* **8** 47.
- ZHANG, Q. C., PETREY, D., DENG, L. et al. (2012). Structure-based prediction of protein–protein interactions on a genome-wide scale. *Nature* **490** 556–560.
- ZINZEN, R. P., GIRARDOT, C., GAGNEUR, J. et al. (2009). Combinatorial binding predicts spatio-temporal cis-regulatory activity. *Nature* **462** 65–70.